Norfolk Boreas Offshore Wind Farm

Norfolk Boreas

Seabed Mobility Study

Applicant: Norfolk Boreas Limited
Document Reference: ExA.AS-2.D1.V1
Deadline 1

Date: November 2019
Revision: Version 1
Author: Vattenfall

Photo: Ormonde Offshore Wind Farm

Monday 25th November 2019

NORFOLK BOREAS OFFSHORE WINDFARM

For the Attention of the Examination Panel for Norfolk Boreas Offshore Windfarm (EN010087) and the Marine Management Organisation and their scientific advisors.

The following information has been redacted from the Norfolk Boreas - Geophysical Seabed mobility assessment. This report was requested for Submission at Deadline 1 (25th November 2019) during Issue Specific Hearing 2 (14th November 2019) of the Norfolk Boreas Offshore Windfarm Examination.

Page 9, Footnote. Commercially sensitive information showing the layouts investigated, used in Vattenfall internal business case.

Page 54, Table 15: Layouts Investigated for this report. Commercially sensitive layouts used in Vattenfall internal business case.

Page 55, Figure 44: Confidential Layout plot on Fugro 2017 Bathymetry. Commercially sensitive information showing locations and numbers of potential turbine positions under Layout XXXXXXXX used in Vattenfall internal business case. Also redacted from contents page.

Page 56-58, Table 17: Confidential Layout predictions for global seabed changes. Values in [m]. Commercially sensitive information showing coordinates and numbers of potential turbine positions under Layout XXXXXXXX used in Vattenfall internal business case.

Page 59, Figure 45: Confidential Layout plot on Fugro 2017 Bathymetry. Commercially sensitive information showing locations and numbers of potential turbine positions under Layout XXXXXXXX used in Vattenfall internal business case. Also redacted from contents page.

Page 60-62, Table 18: Confidential Layout predictions for global seabed changes. Values in [m]. Commercially sensitive information showing coordinates and numbers of potential turbine positions under Layout XXXXXXX used in Vattenfall internal business case.

Page 63, Figure 46: Confidential Layout plot on Fugro 2017 Bathymetry. Commercially sensitive information showing locations and numbers of potential turbine positions under Layout XXXXXXX used in Vattenfall internal business case, also redacted from contents page.

Page 64-66, Table 19: Confidential Layout predictions for global seabed changes. Values in [m]. Commercially sensitive information showing coordinates and numbers of potential turbine positions under Layout XXXXXXX used in Vattenfall internal business case.

Page 67, Tables 20-23. Commercially sensitive information showing the classification of seabed positions including confidential layouts, zones and design criteria

Page 69, Section 9 Conclusion. Commercially sensitive information identifying possible layouts.

Page 68. A list of attached (digital) supporting appendices shown in this section (7.7). These appendices contain commercially sensitive data used to produce the redacted figures and charts listed above.

Norfolk Boreas - Geophysical Seabed mobility assessment

Morphodynamic study

Confidentiality class: High (C3)

Document control

Type of document	Document identification	Rev. No.	Document issue date	Livelink doc.
Report	-	2	12-09-2019	-
Author(s)				
Mikkel Klahn				
Reviewed by		**Approved by**		
J. Hine		A. Galbraith		

Revisions

Rev No.	Date	Revised by	Approved by	Changes
0	15/4-2019	MK		Prepared for internal revision
1	23/4-2019	MK		Updated for revised layouts
2	21/6-2019	MK	AG	Internal revision completed

Report Glossary and Definitions

ALARP	As Low as Reasonably Practicable
BE	Best Estimate
BH	Geotechnical Borehole
CPT	Cone Penetration Test
CPTU	Cone Penetration Test (u: pore pressure)
CTD	Chart Datum
DGPS	Differential GPS
DPR	Daily Progress Report
DTM	Digital Terrain Model
EAOW	East Anglia Offshore Wind farm
ETRS89	European Terrestrial Reference System 1989
GIS	Geographical Information System
HAT	Highest Astronomical Tide
HSBL	Highest Sea Bed Level
km	Kilometre
LAT	Lowest Astronomical Tide
LSBL	Lowest Sea Bed Level
MAG	Magnetometer
MCS	Multi-Channel Seismic
MBES	Multi Beam Echo Sounder
mbsb	meters below seabed
NB	Norfolk Boreas
OWFZ	Offshore Wind Farm Zone
SBES	Single Beam Echo Sounder
SBP	Sub Bottom Profiler
SI	International system of units
SVP	Sound Velocity Probe
SSS	Side Scan Sonar
UHRS	Ultra High Resolution Seismic
UTM	Universal Transverse Mercator
UXO	Unexploded Ordnance
QA	Quality Assurance
QC	Quality Control
VC	Vibrocore
VORF	Vertical Offshore Reference Frame
WGS84	World Geodetic System 1984 (EPSG:4326)
WTG	Wind Turbine Generator

Contents

1. Introduction

In the ongoing development of the Norfolk Boreas Offshore Wind Farm Zone Vattenfall Vindkraft A/S was requested to produce a morphodynamical desk study based on available geophysical and geotechnical information. The geographical extend of the Site is illustrated in Figure 1. All coordinates stated from this point on, unless otherwise specified are reduced to *ETRS89 UTM31N* (See Table 1 for more details).
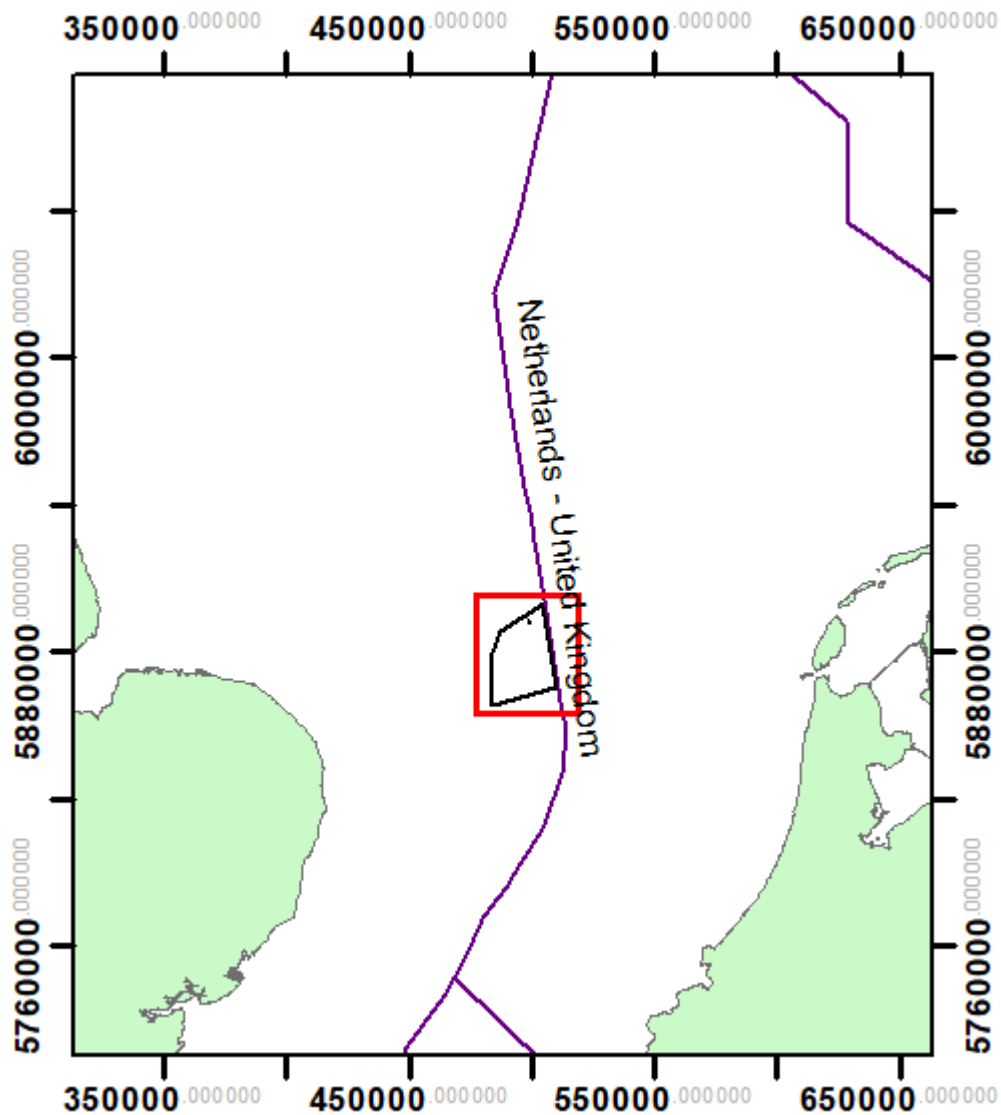

Figure 1 Map showing the location of the planned Norfolk Boreas Offshore Wind Farm Zone within the red polygon.

The area designated for construction of the wind turbines (WTGs) is illustrated in Figure 1, and is located approximately 80 km off the Norfolk East-coast. The area is dominated by a prevailing North-South tidal current[1] defining the formation of regional sediment structures and depositional / erosional patterns[2]. This report aims to

1.1. Previous studies

The Norfolk Boreas site, previously part of the East Anglia Offshore Wind Farm zone (EAOW), has been investigated by a number of studies[2–5] whilst part of the EAOWZ, Additional studies were completed following the division of the site into the Norfolk Vanguard (East and West traches)[1,5,6] and the Norfolk Boreas[4,5,7] sites.

The zonal MBES coverage obtained by Gardline in 2010 is illustrated in Figure 2.
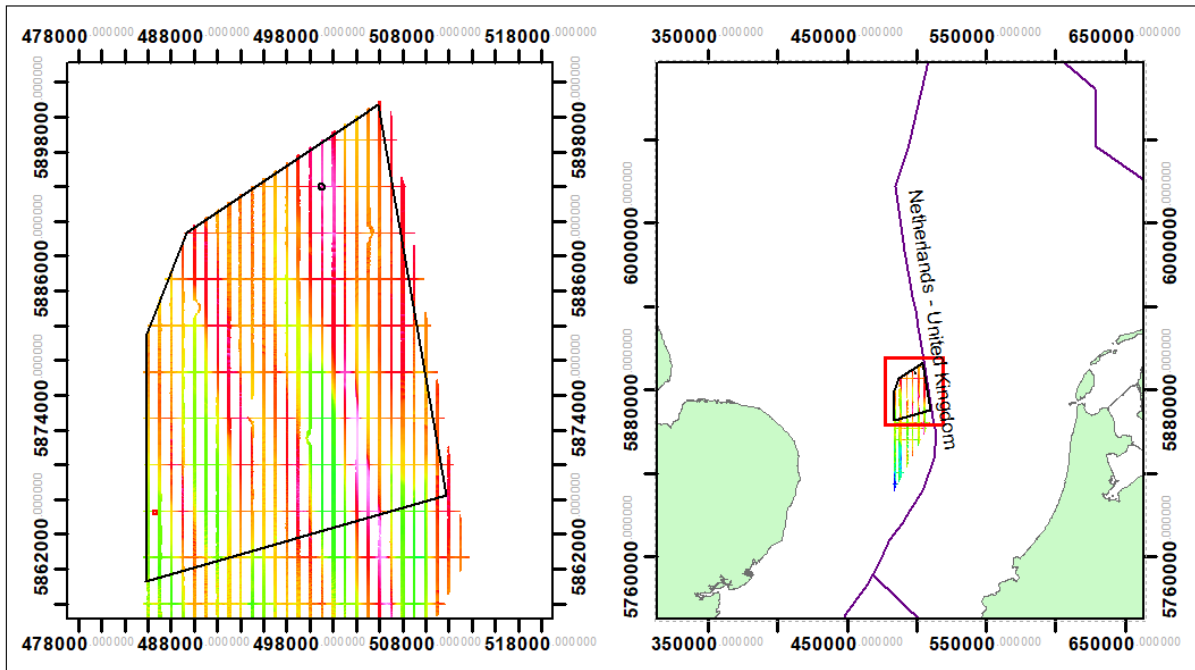

Figure 2: Gardline 2010 MBES coverage. Black line indicating the Norfolk Boreas site boundary[1].

It is readily established that seabed features ranging from mega ripples to sand waves should be considered mobile[5,8–10], an example is illustrated in Figure 3, showing the displacement of 2 sand-waves between 2010 and 2017.This report aims to provide greater detail in terms of quantifying the mobile regime regarding its vertical variability at all points throughout the discrete area constrained by the 2017 MBES data.

Figure 3: Gardline 2010 MBES data overlaying Fugro 2017 MBES. Side-length 500 x 500m.

---

[1] Vattenfall GIS ID: UNB_BDSB_SiBdry_v01_180326fi_25831

Norfolk Boreas - Geophysical Seabed mobility assessment
Morphodynamic study
    Confidentiality class: High (C3)   6 (72)

1.2. 2017 Site Investigation

Fugro acquired site investigation data (MBES, SSS, MAG, SBP, 2DUHR, CPT's, VC and BH) within the proposed NB (Norfolk Boreas) Wind Farm Site in 2017. Additionally, MBES (Multi Beam Echo Sounder) data was acquired to monitor sediment mobility at the beginning of 2016. The additional sediment mobility survey coverage is shown in the upper left frame of Figure 5 and is indicated by the red polygon in Figure 4. Findings will be further correlated with the geotechnical assessment carried out by Fugro[11].

The 2017 MBES survey coverage overlain by the 2016 pre-investigation (red polygon) is illustrated in Figure 4.
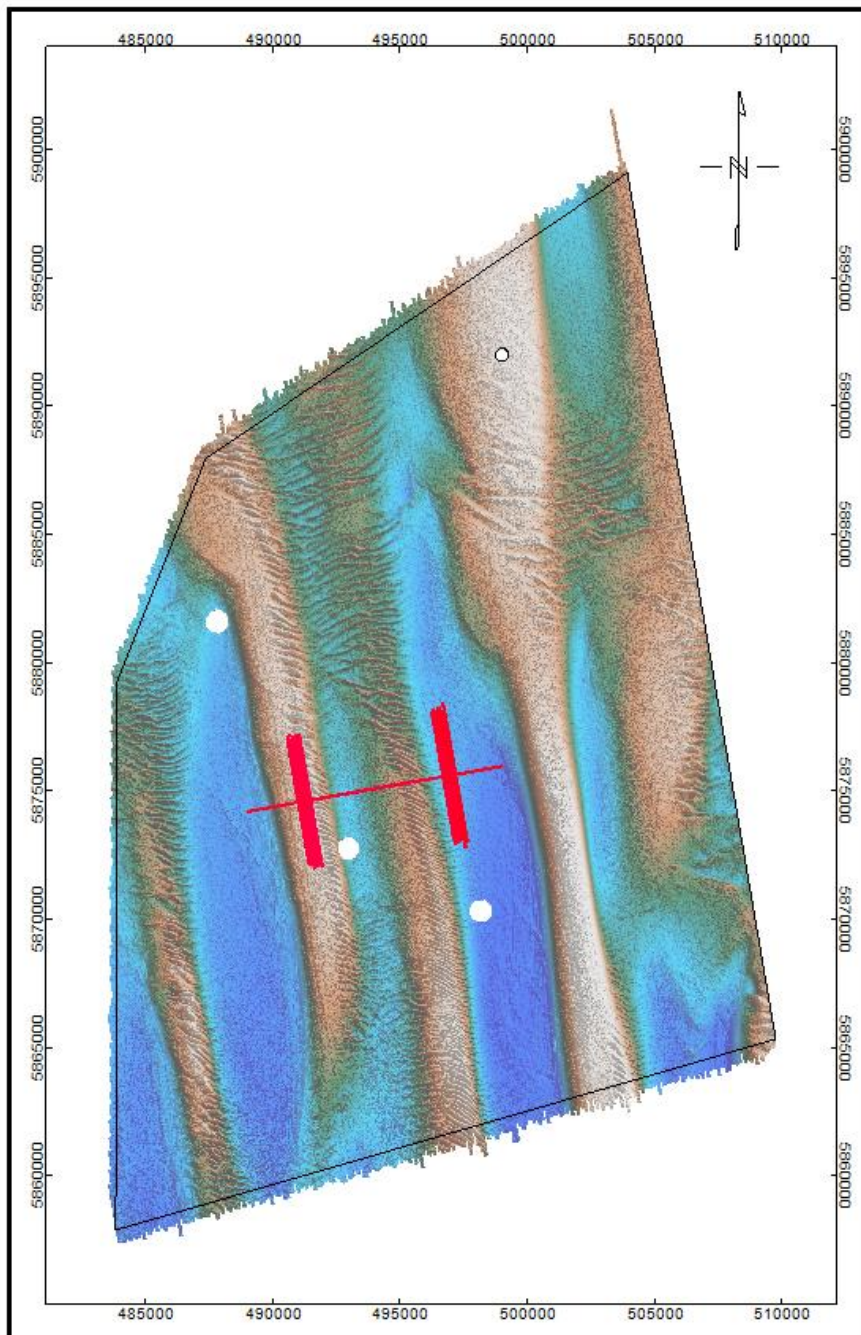

Figure 4: Norfolk Boreas 2017 MBES coverage. Black outline illustrating the site-boundaries.

An example of year-over-year movement for a single sand-wave is illustrated by Figure 5.
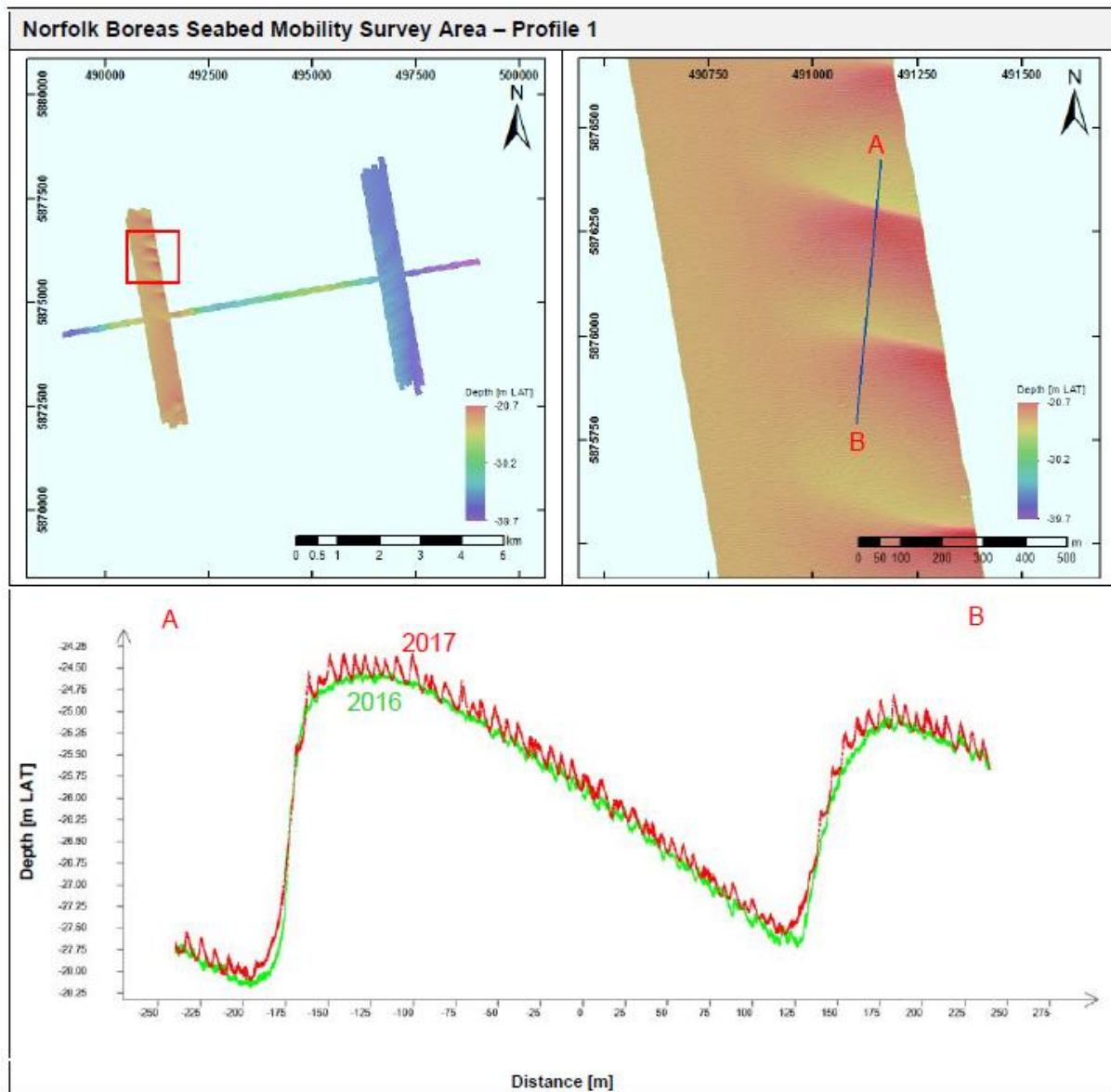

Figure 5: 2016 - 2017 seabed comparative cross-section. Figure by Fugro[5].

As shown in Figure 5, the (partially) illustrated sand-wave (uppermost right frame) strikes East-West with a steep northwards dip. No significant lateral displacement of the sand-wave-crests are observed in Figure 5, although the superimposed mega-ripples illustrate some degree of mobility. Several figures were produced by Fugro[5], they all displayed similarly little wave-crest displacement..

1.3. Objectives and deliverables

As identified by DNV-GL-ST-0437 section 2.5.9.c [12] it is critical to identify mobile structures, i.e. sand bars, sand waves, ripples etc. throughout an offshore wind farm zone. DNV-GL-ST-0126 section 8.1.1.1 [13] acknowledges the importance of global seabed changes, i.e. site-specific geomorphology, which this report aims to address by comparing the 2010 bathymetry to the 2017 bathymetry.

Furthermore, this report aims to clarify bathymetrical site conditions in accordance to DNV-GL-SE-0190 [14] in order to be included in the design-works for the Norfolk Boreas Offshore Wind Farm.

To summarise, this report will comprise the following information:
- A detailed description of morphodynamical features within the wind farm zone.
- An analysis of morphodynamical features.
- An extrapolation of recent morphodynamical activities to estimate future changes caused by migrating bedforms.

To support the morphodynamical analysis and predictions made based on the bathymetrical breakdown, geological, geophysical, geotechnical, and hydrodynamic conditions will be considered. Predictions for potential seabed changes (sedimentation / erosion) will be based on an extrapolative seabed forecast by transposing the 2017 bedforms according to several factors, to be discussed in section 7, page 33.

Deliveries based on this analysis will be presented as:
- This report, detailing the outcomes of the conducted analysis and main results.
- A Microsoft Excel Spreadsheet listing the range of expected change for each WTG position[2].
- Best-estimate seabed grids for every 5-year period following 2020.

1.4. Report structure

This report will be organised into the following sections:

1. Introduction to the project, data overview, and objectives.
2. Background information for data used in this report.
3. Introduction to the Norfolk Boreas geological framework.
4. Seabed classification
5. Hydrodynamic conditions and their potential impact on specific lithology and thus morphodynamical entities
6. Bathymetrical data and classification of seabed structures.
7. Morphodynamical model setup & application.
8. Future work prospects.
9. Conclusions based on the conducted analysis.
10. References

---

2 ▮▮▮

The primary emphasis of this report will be section 7, as this analysis unites the main objectives, as per section 1.3, and will comprise the analysis of existing features and the prediction-model for any natural geomorphological changes expected throughout the lifespan of the windfarm.

1.5. Report Geodetic and projection parameters

All surfaces and coordinates in this report have been reduced to a uniform projection to allow for full comparability, details stated by Table 1.

Table 1: Geodetic and projection parameters.

Local Datum Geodetic Parameters	
Datum	European Terrestrial Reference System 1989 (ETRS89)
Spheroid	GRS80
Semi Major Axis	a = 6 378 137.000m
Inverse flattening	1/ f = 298.257 222 101
EPSG Code	6258
Project Projection Parameters	
Grid projection	Universal Transvers Mercator (UTM)
UTM Code	31 Northern Hemisphere (31N)
Central Meridian	003° 00' 00.000'' East
Latitude of Origin	00° 00' 00.000'' North
False Easting	500 000 m
False Northing	0 m
Scale factor on central meridian	0.9996
Units	Meter
EPSG Code	25831

Notes:

Any data received using other projections and/or reference systems have been converted to the in this table stated projection and reference (ETRS89 UTM31N).

The shift has been made using Oasis Montaj 9.3.1.

2. Background information

The following sections of the report provide details based on the data analysis and categorise identified bedforms based on their amplitudes and wavelengths.

2.1. Data basis

To inform this study various data-sources were included. The Vattenfall Metocean Group provided a time series comprising current- and wave-model-data at 2 distinct locations within the Norfolk Boreas OWFZ (Figure 6). The modelled data-series begins on March 1st, 1979 through December 31st, 2017, data resolution being 20 minutes and 60 minutes for currents and waves respectively.
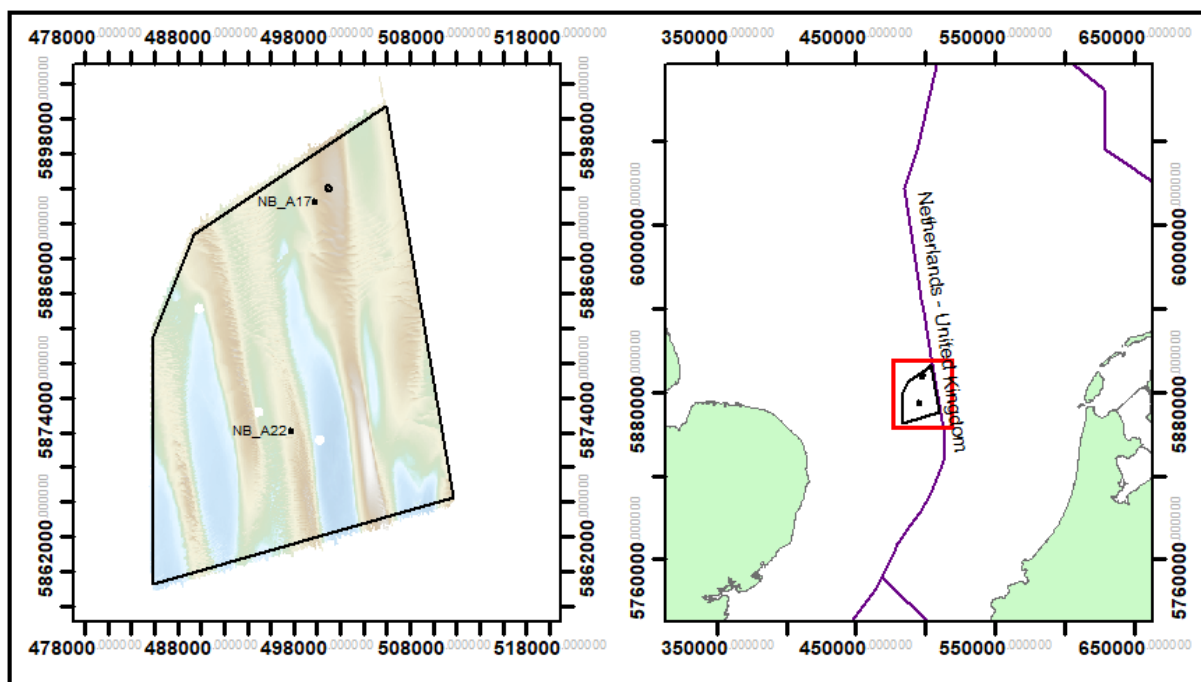

Figure 6: Metocean measurement locations.

The locations displayed in Figure 6 are detailed in Table 2 below.

Table 2: Metocean input sources.

ID	X	Y	Wave Data Source	Hydrodynamic Data Source
NB_A17_Metocean_53p166N_2p968E	497861	5890737	MetoceanWorks Swan Model	MetoceanWorks MIKE21 Model
NB_A22_Metocean_52p989N_2p937E	495771	5890737	MetoceanWorks Swan Model	MetoceanWorks MIKE21 Model

All bathymetrical surveys data available at the time of writing this report are summarised in Table 3.

Table 3: Survey Overview.

Year	Surveyor	Survey Method	Data density	Coverage	Used in this study
2010	Gardline	MBES	High	Mesh-grid comprising MBES data covering	Yes
2016	Fugro	MBES	High	Low, reoccurring reconnaissance survey	No
2017	Fugro	MBES	High	Full coverage of the NFV OWF West site	Yes

The geographical extend of the MBES datasets is illustrated by Figure 7 below.
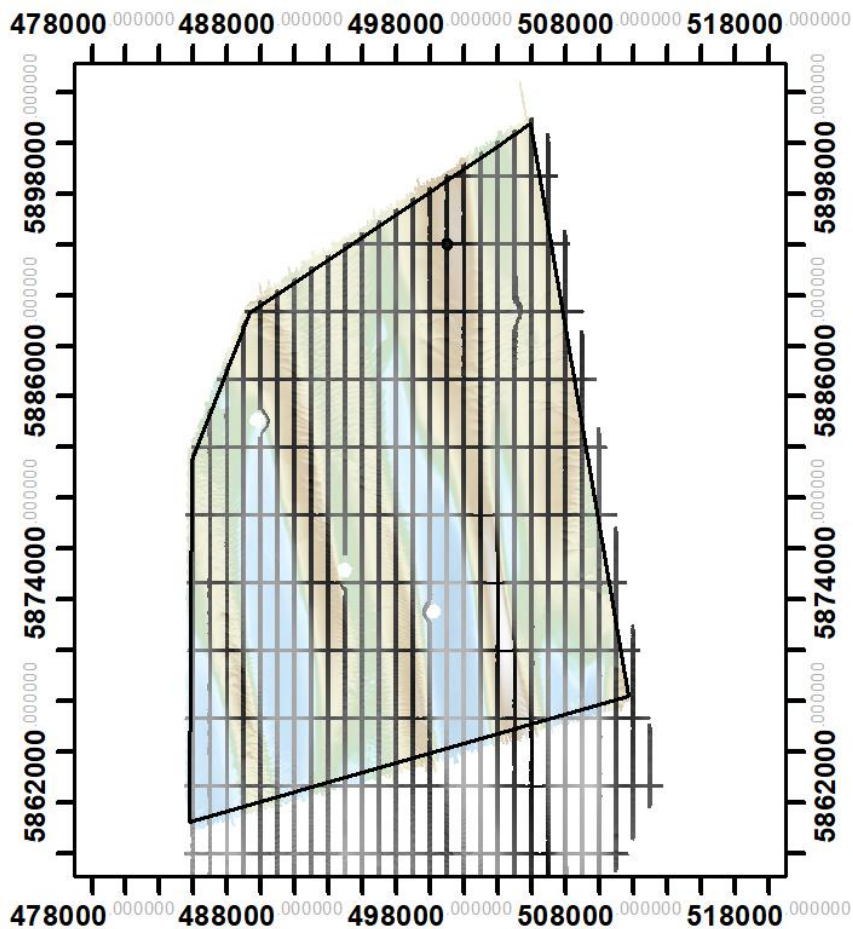

Figure 7: Gardline 2010 bathymetry (grey mesh) overlaying the bathymetry measured by Fugro in 2017.

The spatial overlap between the datasets used for the analysis (2010 over 2017) has been calculated.

Shared coverage	**31%**
Overlapped cells 2010 (5x5m)	9.388.146
Total cells 2017 (5x5m)	30.320.430

This overlap is considered significant given that a Confidence level of 99% with a confidence interval of 0.01 can be achieved using this sample size. Hence the overlap is considered valid for further comparative analyses.

The bathymetries have been gridded for the analysis as detailed in Table 4. All gridding is performed by Geosoft Oasis Montaj 9.3 and Global Mapper 19.

Table 4: Performed gridding.

Year	Point spacing	Gridding method	Cell Size	Description
2010	1 m	Minimum curvature	1.0 m 5.0 m	0 blanking distance to avoid extremes at or around the grid-edges. 5m cell-size export from Global Mapper to Oasis Montaj.
2017	0.25 m	Minimum curvature	1.0 m 5.0 m	Cell-size set to 1m to ease processing. The full site at 0.25m resolution exceeds the memory-allocation. 5m cell-size to smooth out short wavelength noise.

As the geological context is vastly important to the erodibility of underlying sediments and thus partially controls the potential rate of seabed change, it is important to include any such data in the evaluation of the prediction model to avoid overly conservative estimates. This is done by checking the depth (mbsl) to the base of unit A[1] (Holocene sand, Table 5) using the 2017 Fugro SBP & UHR survey data, the Unit A isochore map is illustrated in Figure 8. The interpreted isochore grid is subject to the resolution in the SBP data, i.e. a 100m line-spacing, hence no minute details should be interpreted from this map. From Figure 8 it can be identified that Holocene sediments are distributed in a longitudinal pattern oriented ~ N-S.

Further gridding is performed to build up the prediction model, this will be discussed in section 7.
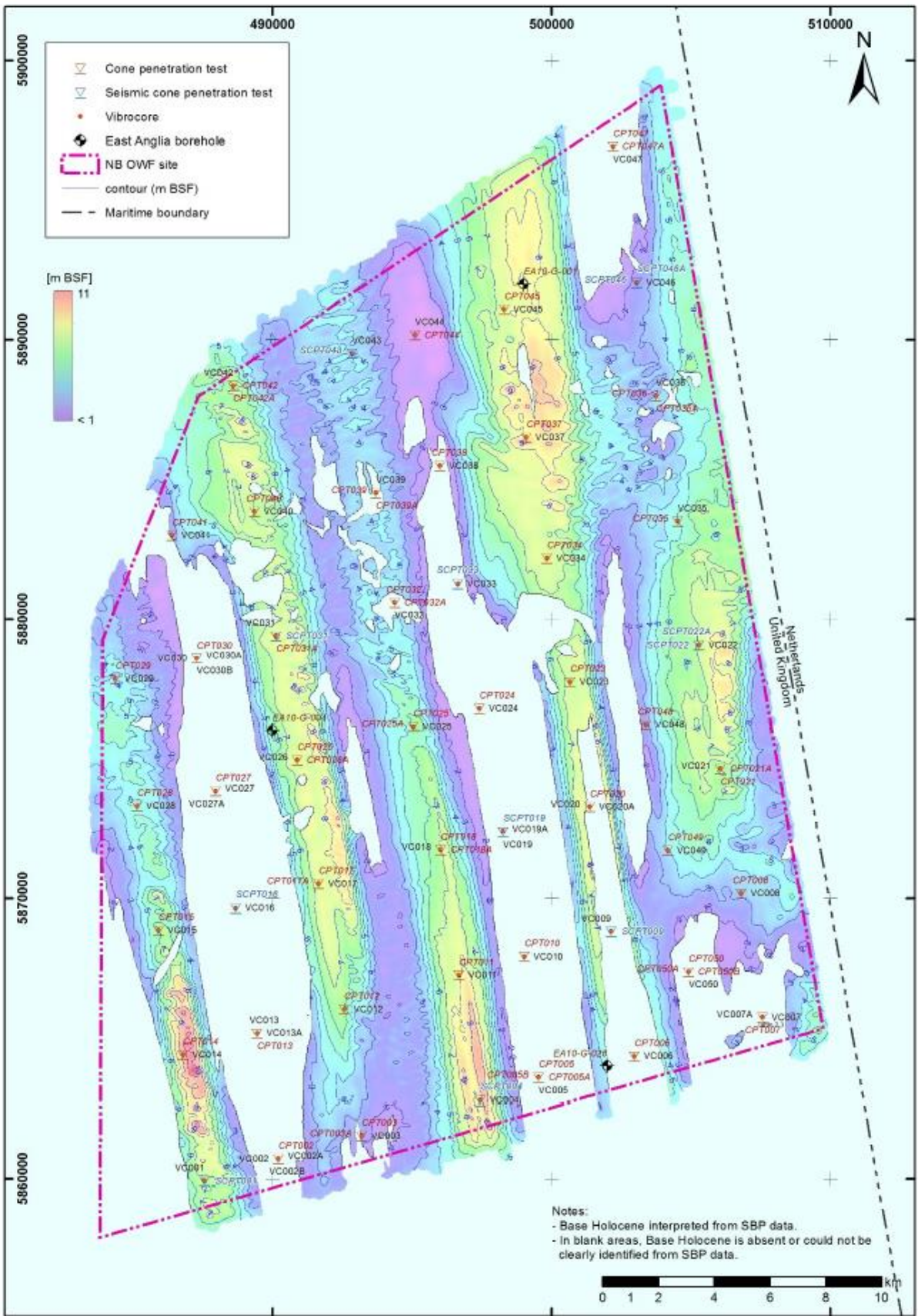
Figure 8: Unit A isochore map, figure by Fugro 2018.

2.2. Classification of morphodynamical seabed features

Large parts of the North Sea, this site included, are covered in a systematic pattern of rhythmically distributed bedforms. These features are the sum of influencing parameters, i.e. hydrodynamics, sediment transport, local sediment sources as well as the underlying geological constitution[3,15–21].

The indication of changing environments is often illustrated by aggrading or erosional trends in the cumulative subsurface[22–28]. The significance of such variations is a result of changing hydrodynamics, variations in sediment supply or long-term eustatic changes[26,29]. In marine basins, such as the North Sea, sediment is transported by a variety of subaqueous currents[18,20,30,31]. The environment governing the NB Site suggests residual tidal currents (± 25° NNW - NNE) to be the driving force as no significant nearby sediment supply, i.e. large river-estuary is feeding the area[18,26,32].

This Site features several morphological seabed structures. The smallest measurable features being ripples but given their height and wavelength in the range of a few centimetres they are generally considered insignificant for both cable-installation and WTG-foundations. Mega-ripples, while architecturally like *Ripples* in terms of amplitude to wavelength ratios, are 1 - 2 orders of magnitude larger than their smaller counter-part, feature amplitudes in the range of decimetres to ~1m [18].

Sand waves cover large parts of the shallow seas, such as the North Sea, and generally form a distinctive pattern with crest-spacing in the range of 100s of meters to around 1 km. Crests are assumed to be perpendicular to the principal current, only deviating ± 10° [20]. Lateral movement of sand waves is thought to be structurally significant throughout the lifetime of a wind farm (25 years), with lateral movement perpendicular to the crest-line being able to exceed 25 m p.a. [18]. The amplitude of sand-waves and their dynamic properties causes them to be considered a possible major hazard to offshore constructions (amplitudes ranging from 1 to several meters) and thus a design-impacting feature to be considered.

Lastly, sandbanks / tidal bars are vast features with dimensions large enough to be considered significant for wind farms, however their rate of movement is very limited and they can be considered stationary throughout the lifetime of a windfarm[18].

While considered insignificant in terms of general water depth, small-scale features (sand-sheets, small ripples, etc.) migrate at a much larger pace, and thus account for a significant volume of the actual sediment transport[17]. Therefore, it is considered important assess the seabed roughness (bedforms superseding sand-wave-scale structures) to improve the understanding of site-specific migration patterns.

Deltares[18] have created a risk diagram assessing seabed structures in terms of their impact on WTG foundations (Figure 9) which suggests the primary hazard to structures to be sand waves, with mega ripples and sand banks being a minor hazard.
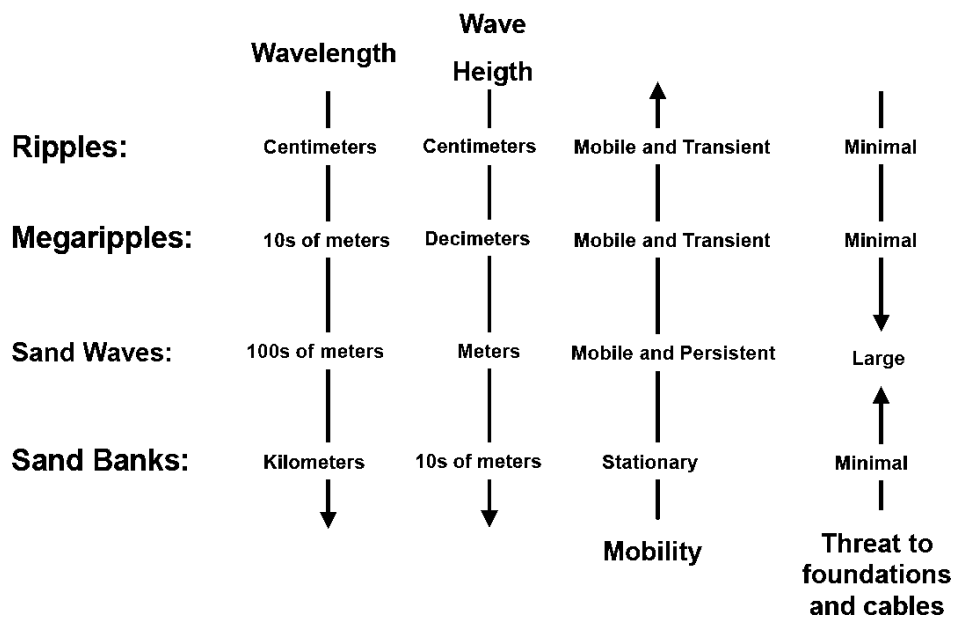
Figure 9:Seabed feature threat-classification. Classification by Deltares[18].

2.2.1. Sand-wave considerations

As illustrated in Figure 9 sand-waves pose the most imminent threat to the WTG foundation during its lifetime, which emphasises the importance of gaining an in-depth understanding of the regional setting regarding the morphodynamical characteristics of sand waves.

It has been proposed that sand waves can migrate in oscillating directions under normal circumstances[33], as well as crest characteristics deviating from their general cross-current orientation when in close proximity to sub-aqueous channels featuring higher flow velocities[34]. Sand-wave studies, i.e. steady state models held up against real-world measurements, suggest residual currents are responsible for sheer migration whilst the prominence of oscillating currents define the actual formation characteristics. The migration velocity is tied to the surface shear stress[20] which affects the viscous mediums (waters) ability to suspend particles, this force largely correlates with the flow-velocity. Further parameters considered by Nemeth et. al [20] are asymmetrical tidal currents, and slope-properties. The unconsolidated sediment composition further influences the overall structural stability of the seabed in certain hydrodynamic regimes [21].

The exact modelling of sand wave migration requires a very detailed dataset with very high temporal resolution. The sum of all parameters is presented by the regional seabed morphology, and a general prediction will therefore be based on analysis of the bathymetrical data.

The sand wave crests have been mapped, and the migration velocity has been assumed to be constant, with migration occurring at the average rate observed between 2010 and 2017. Employing the 1979 – 2017 hydrodynamic observations and observed sand-wave strike-dip orientation to establish the imposed direction of migration a vector-field will be created to transpose the sand waves once isolated from the underlying bathymetry. It is henceforth assumed that no significant wave-form alteration will be introduced throughout the life-time of the windfarm[18].

3. Geological setting

As described in section 2 the geological context establishes part of the key framework for any dynamic seabed, as the material comprised in the subsurface ultimately must be sufficiently unconsolidated to form dynamic structures, i.e. structures exhibiting significant year on year migration. The base-level for mobile features has historically been a widely debated topic[35]. Long term changes (thousands to millions of years) will disregard any consolidation and re-establish a stable base-level. In short term 10s to 100s of years the observable trough-levels can be considered a defining base of potential sand-wave erosion[18,20,21,26,32].

The geological overview of the NB OWF Site is summarised by Table 5.

Table 5: Seismo-stratigraphic layering NFV, summarized by Fugro[4] and RIL[3], rendered by Vattenfall.

Seismic Unit	Unit Seismic Signature	Indicative Lithology	Depositional environment	Formation name	Age
A1	Structureless	Fine to coarse sand	Marine	Blight Bank	Holocene
A2	Parallel, draped (into small channels), high amplitude	Fine sand and clay	Lagoon, swamp	Elbow	
B	Structureless	Fine sand	Periglacial, aeolian	Twente	Late Weichselian
C	Continuous, finely laminated, horizontal	Silty, sandy clay	Brackish marine	Brown bank	Late Eemian to Early Weichselian
E	Structureless or transparent	Unknown	Sub-glacial	Swarte Bank	Elsterian
F	Chaotic, structureless, imbricated	Fine to medium sand	Fluvial (delta plain)	Yarmouth Roads	Waalian to Early Elsterian
G	Typically, chaotic, some prograding reflectors	Fine to medium sand	Fluvial to shallow marine	Winterton Shoal	Eburonian to Waalian

The Quaternary deposition and erosion in the area has generally been controlled by shifting ice-ages and the associated eustatic sea-level changes, i.e. vast unconformities are known to have developed across the site[3].

The lithological units present in the substrate (Table 5) were laterally resolved by UHRS data[3,4]. The 2017 line-plan is illustrated in Figure 10, showing a tight line-grid (100m inline-spacing) which was acquired across the site.
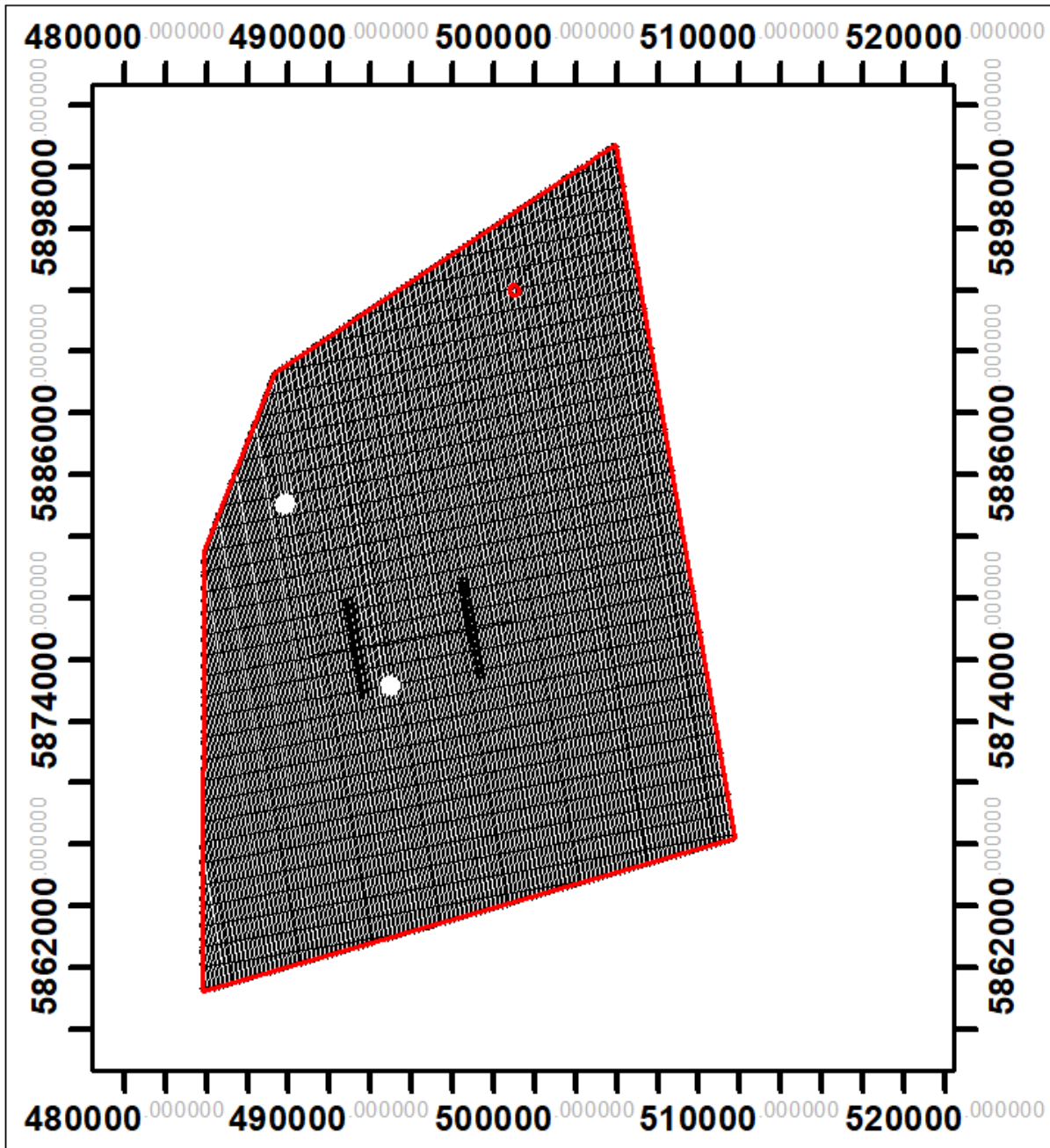
Figure 10: Fugro 2017 proposed UHR & SBP line-plan[4].

The importance of the uppermost strata (0 – 10m bsb) is emphasized by Figure 11, which illustrates bedforms shorter than 800m identified on-site (grey-toned layer) overlaying the Holocene sediments[4]. This shows a strong correlation between the Holocene Sands and the presence of vast, steep sand-wave arrays overlaying larger sand-bodies described as *Tidal Current Ridges*[2]. Hence it is thought, that local sourcing of sediment plays a significant role in the formation of the mobile bedforms on-site[2,36,37].
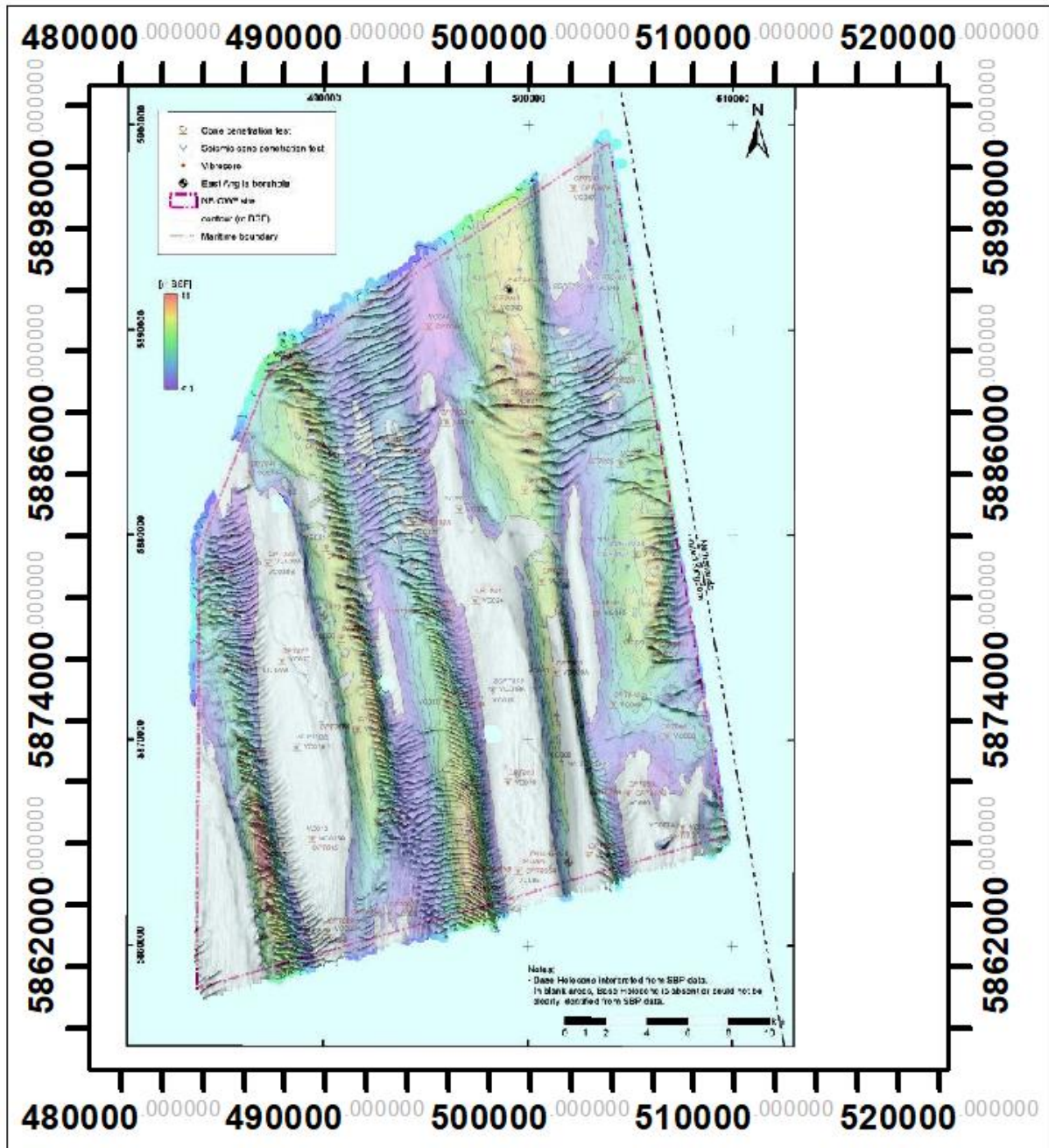
Figure 11: Unit A isochore map overlain by bedforms shorter than 800m (darker shadows = taller bedforms).

Throughout the Upper Pleistocene when the sea level was relatively low[38] the area was part of a periglacial tundra[3]. During the retraction of land-based glaciers unstable landscapes will have been exposed and, thus, prone to reworking[39–42]. The paraglacial processes preceding present-day will have reworked the exposed surface extensively [43] which was later flooded during the Holocene transgression. This led to the formation of tidal ridges once significant tidal currents were established. The requirements to form tidal ridges is thought to be tidal currents in excess of $100 cm\ s^{-1}$, which can leave deep furrows between the ridges[35]. The Holocene transgression, which is arguably still ongoing[44], ultimately moved the coastline to its present-day position, drowning the aeolian deposits and allowing for marine reworking of these deposits.

The variation in the thickness of the overlying sands across the Site is further substantiated by the geotechnical interpretation carried out by Fugro[45]. An overview of the CPT and VC locations is illustrated in Figure 12, showing the high proportion of Sand at the seabed. A cross section showing the interpreted thickness of the Holocene sands from the SBP (Sub bottom profiler) is illustrated in Figure 13.
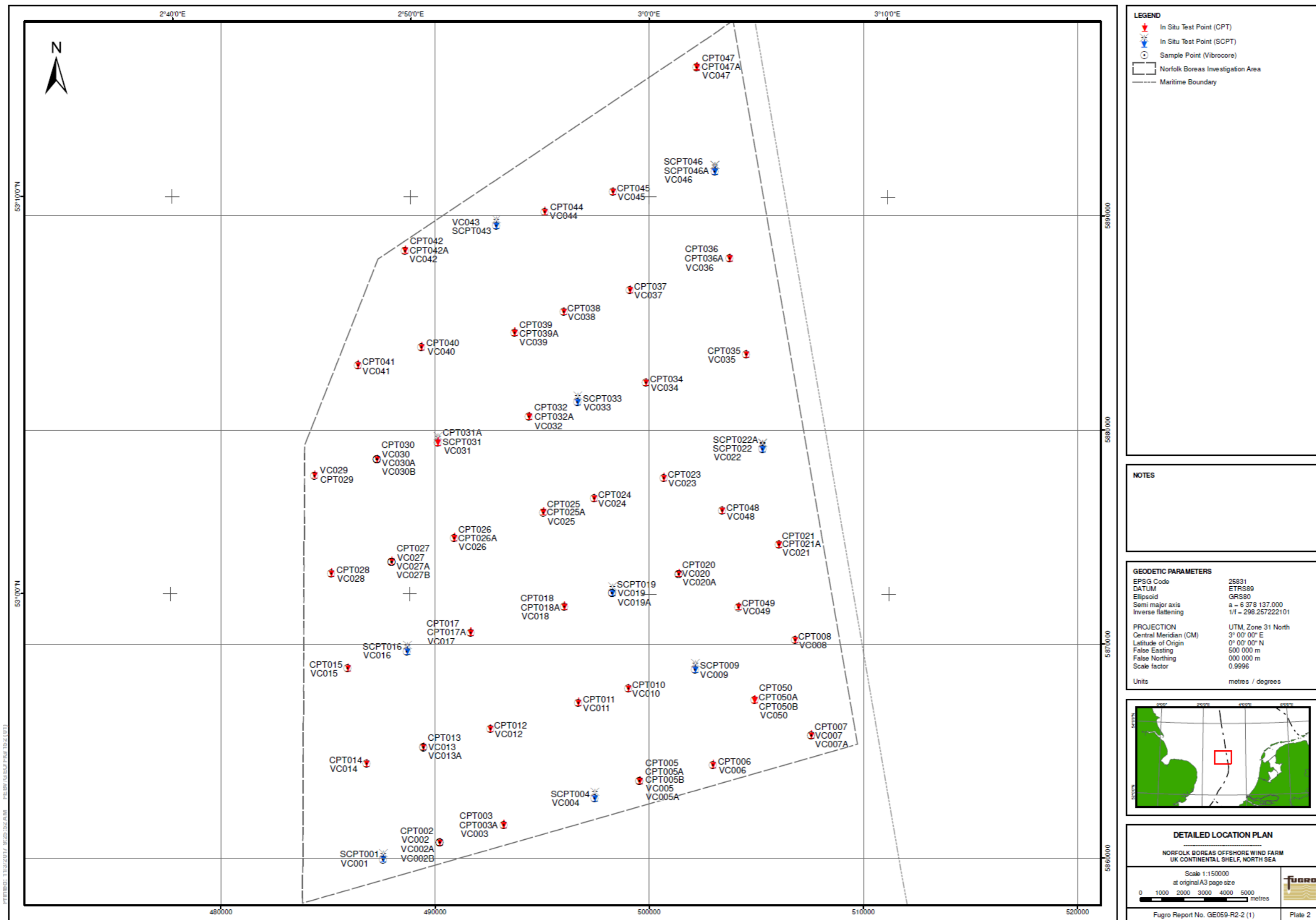
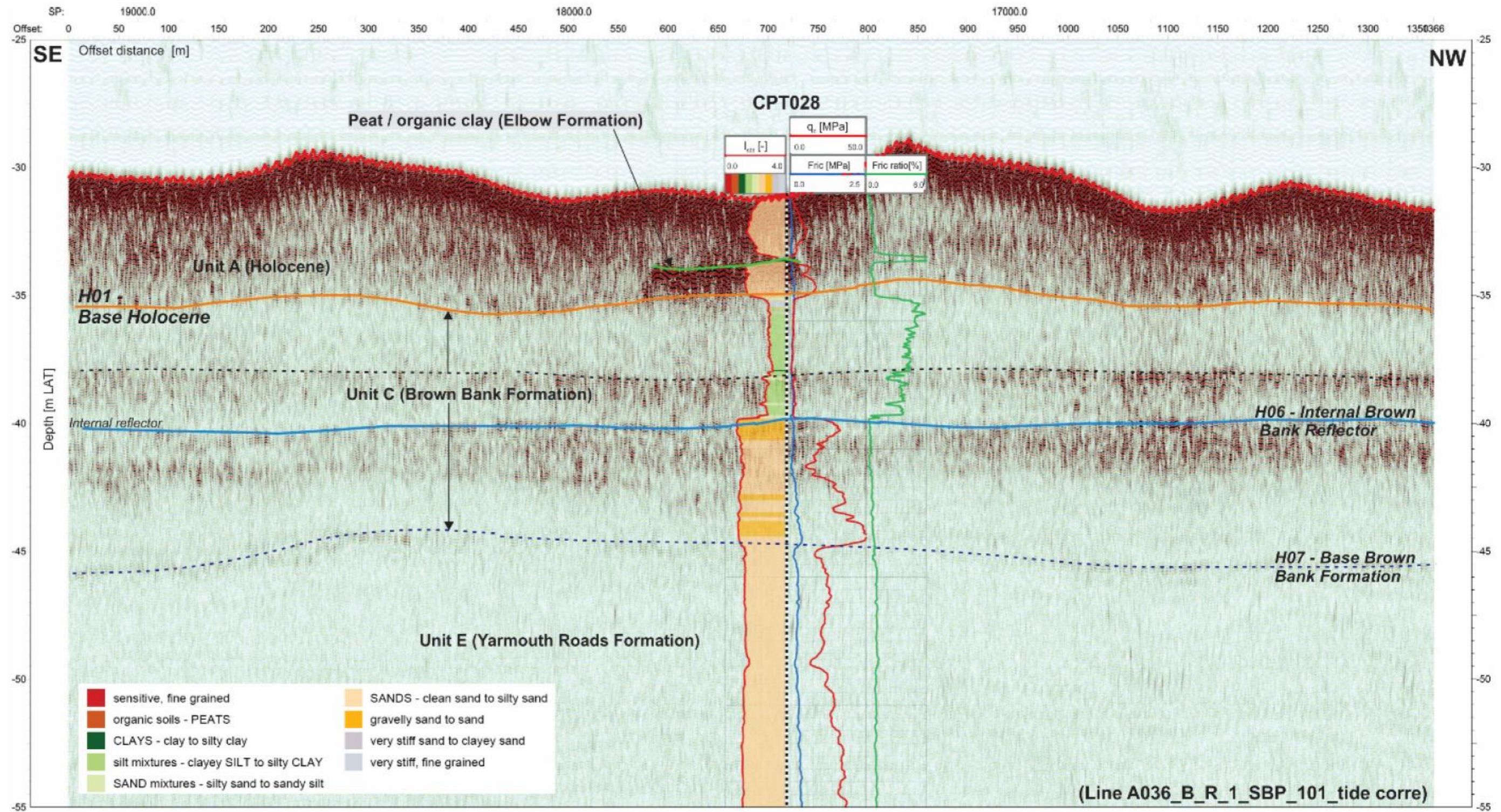Figure 12: CPT & Vibro-core locations from the 2017 Fugro SI. Figure by Fugro 2017[45].

Norfolk Boreas - Geophysical Seabed mobility assessment
Morphodynamic study

Confidentiality class: High (C3)

Figure 13: Cross Section B, CPT interpretation overlaying UHR section. Figure cropped by Vattenfall from Fugro 2017[46].

4. Seabed classification

Fugro[4] provided an overview of VC results (Figure 14). Sediment distribution at the seabed based on the VC's, shows the presence of the beforementioned fine-grained aeolian sands and coarser glacial outwash-sediments from the Holocene glacial retraction. This correlates well with the findings from Fugros CPT's (2016 – 2017[46], Figure 13), suggesting sand-cover at seabed level.

Sand waves are superimposed on the established tidal ridges (sand banks). Some local sub-cropping Quaternary deposits are expected to surface in a patch-like manner. The grain size sorting effect of sand waves has been discussed & modelled in previous studies, I.e. Van Oyen et. Al 2009 [33], which, given the vast sand-waves, is expected to have a distinct impact on grainsizes observed at the seabed[35]. The Quaternary outcrops (Brown Bank)[3] are expected to be resistant to immediate remobilisation given the higher clay-content. Thus, it must be considered that certain features may be stable throughout the lifetime of a windfarm, even though they may be geometrically like sand-waves.
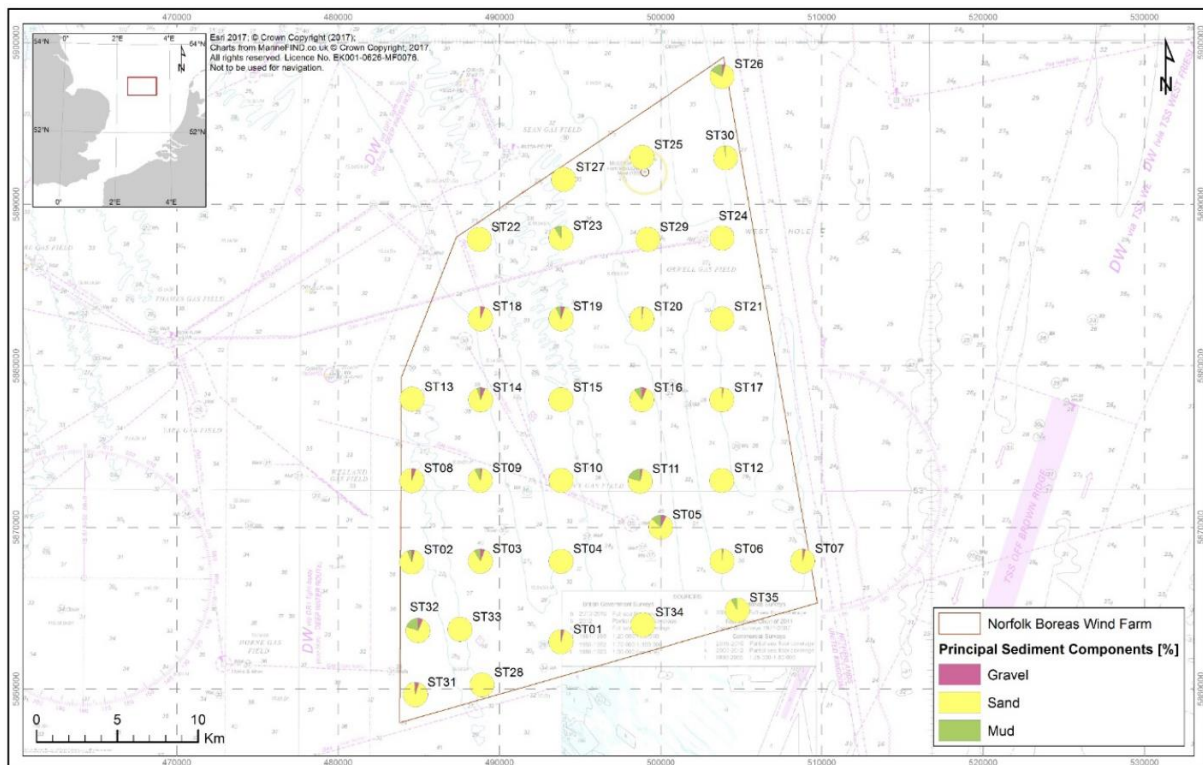

Figure 14 Lithological seabed sampling presented by Fugro[4], Vibro-core-results.

5. Hydrodynamic Conditions

The Vattenfall Metocean Team has delivered current-data for this report. report. The March 1st 1979 – December 31st 2017 current characteristics have been broken down as a rose-diagram detailing the flow direction and intensity for this 38 year model period, illustrated in this report by Figure 15 and Figure 16, for the purpose of this report it is assumed that this timespan complies with DNV-GL-ST-0437 section 3.4.3[12]. As stated by DNV-GL-ST-0437 the variation of current with water depth shall be considered where relevant[12]. The delivered time-series is the depth-average current speed. Current profiles are generally considered logarithmic, with the peak velocities just below sea level [47], as the seabed expresses varying degrees of roughness[17,48] it may be hard to predict exact flow velocities when approaching individual sand-grains at the seabed.

Theoretical current profiles can be established according to Eecen 2010 [47], using the below expression (Equation 1):

Equation 1

$$v(z) = v(0) \cdot \left(\frac{z+d}{d} \right)^{1/7},$$

where $v(z)$ is the current speed at height z and z is the height above sea level (negative in downward direction), $v(0)$ is the current speed at sea level. d is the depth (location of the seabed; taken as a positive number).

As

$$\lim_{d \to 0} v(z) = \varnothing$$

And knowing that in practice $v(z) \to 0$, when $d \to 0$ assuming the subsurface being solid.

To account for this, as well as the increasing Reynolds numbers with increasing seabed-proximity, the depth-average flow velocity is adopted for further analysis.

Peak velocities are expected above the local crests in order to satisfy Bernoulli's Principle[35]. Further, using a dynamic eddy viscosity model the growth rate of sand-waves can be modelled, showing a variation in wave-length and vertical growth-rates based on the level of residual turbulent cells surrounding individual bedforms[37].

As no dynamic current-field has been established, no current-based sand-wave growth will be considered for the purpose of the model presented in the latter sections of this report, rather the assumption is made that wave-forms remain constant throughout the lifetime of a windfarm[18].

To identify the overarching current-regime on-site, the 38-year time-series of modelled currents was evaluated. The summary of these currents is presented by 2 rose-plots; Figure 15 and Figure 16. The location of each individually modelled point is summarized in Table 6.

Table 6: Current-plots

ID	X	Y	Residual direction	Illustration
NB_A17_Metocean_53p166N_2p968E	497861	5890737	North	Figure 15
NB_A22_Metocean_52p989N_2p937E	495771	5871049	North	Figure 16

The locations listed by Table 6 are illustrated in Figure 6 in section 2 of this report.

The NB-A17 current-plot (Figure 15) is situated in the central northern section of the NB OWF Site, and is located some distance (~1km) from bedforms resembling sand-waves.
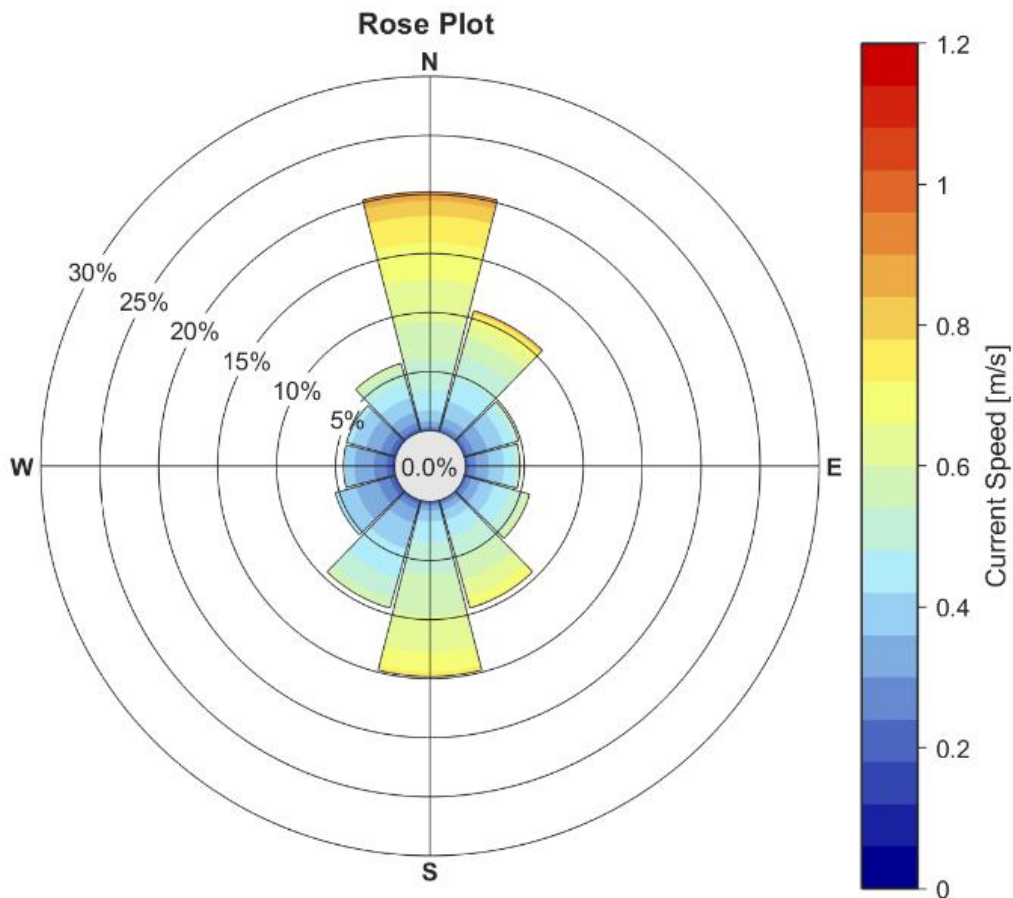
Figure 15: NB_A17_Metocean_53p166N_2p968E, 38 year rose plot.

The NB-22A current-plot, Figure 16, is situated within a field of sand-waves. Currents at this location deviate from the NB_A17 (Figure 15) in terms of residual currents being more profoundly northbound.
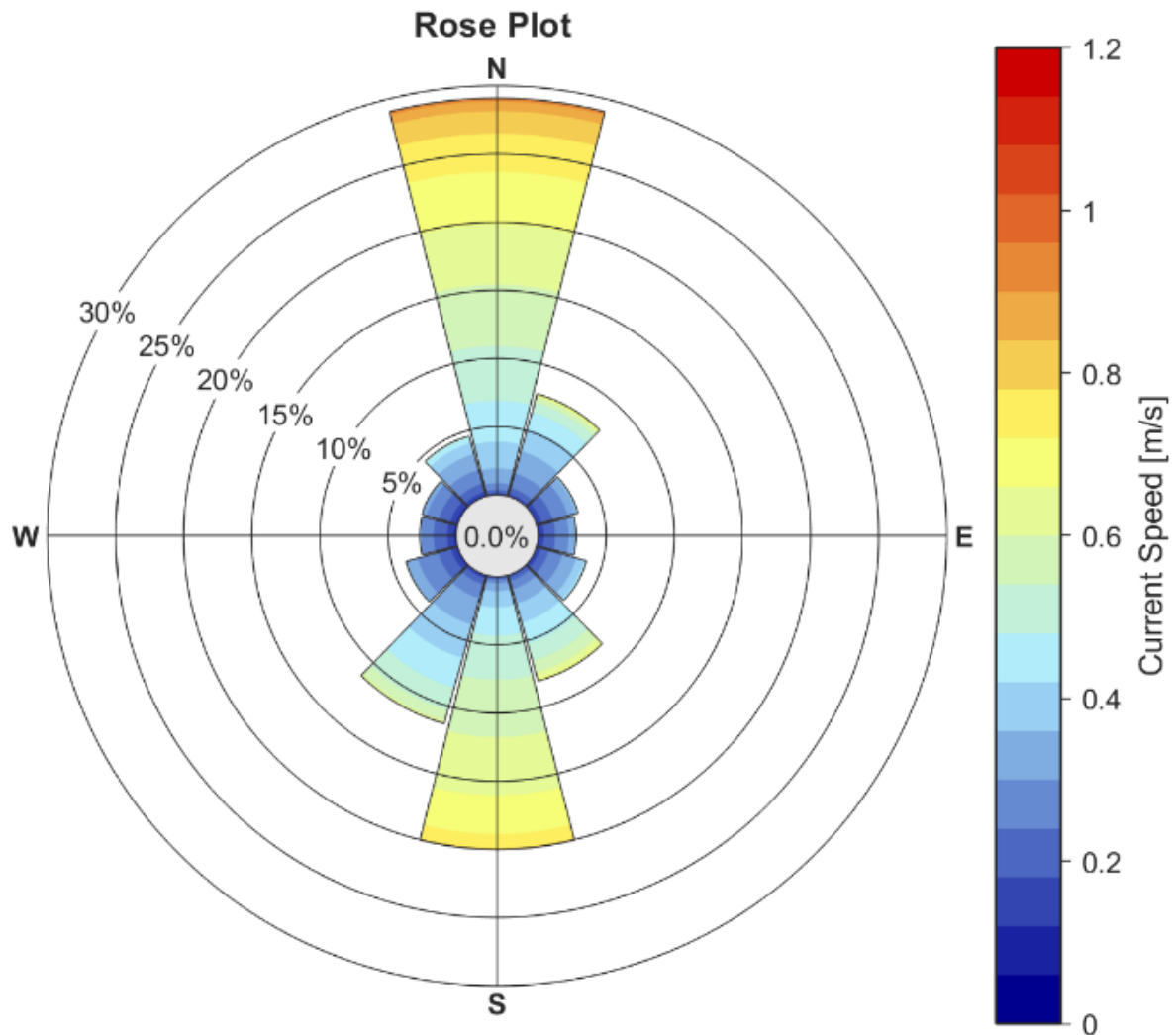
Figure 16: NB_A22_Metocean_52p989N_2p937E, 38year rose plot.

Based on the 2 time-series presented (Figure 15 and Figure 16), omitting the directional component, the intensity of the modelled currents can be analysed for erosional potential (Table 7).

Table 7: Current intensity breakdown.

ID	Minimum (m/s)	Maximum (m/s)	Mean (m/s)	Std. Deviation (m/s)
NB_A17_Metocean_53p166N_2p968E	0.000	1.22	0.48	0.15
NB_A22_Metocean_52p989N_2p937E	0.000	1.17	0.46	0.17

Based on the known flow velocities an assessment of the mobile grain sizes can be made according to the Hjulström diagram [35], Figure 17. For this the NVW_NW location is chosen, as this location shows the most intense current and is situated closest to a sand-wave cluster. Hence, it is considered most representative for this Site.

The mobile regime, which is conceptualised by Figure 17, using the mean-depth current values, insinuates extreme events to mobilise well into the pebble regime, albeit a majority of flow velocities (3 σ) are within the erosional regime comprising medium silt – medium gravel,

suggesting unconsolidated material, i.e. sands and gravel, to be mobilised regularly throughout the lifetime of an OWF (25 years).

A graphical representation of this is illustrated by Figure 17. The Hjulström Diagram shows the relationship between flow velocities and erodibility of sediments of certain grain size. This suggests Clay to have a stabilising and / or consolidating effect on the seabed. While Figure 17 illustrates the extreme case assuming no loss of directional velocity, it helps to conceptualise the relationship between currents and erodibility.
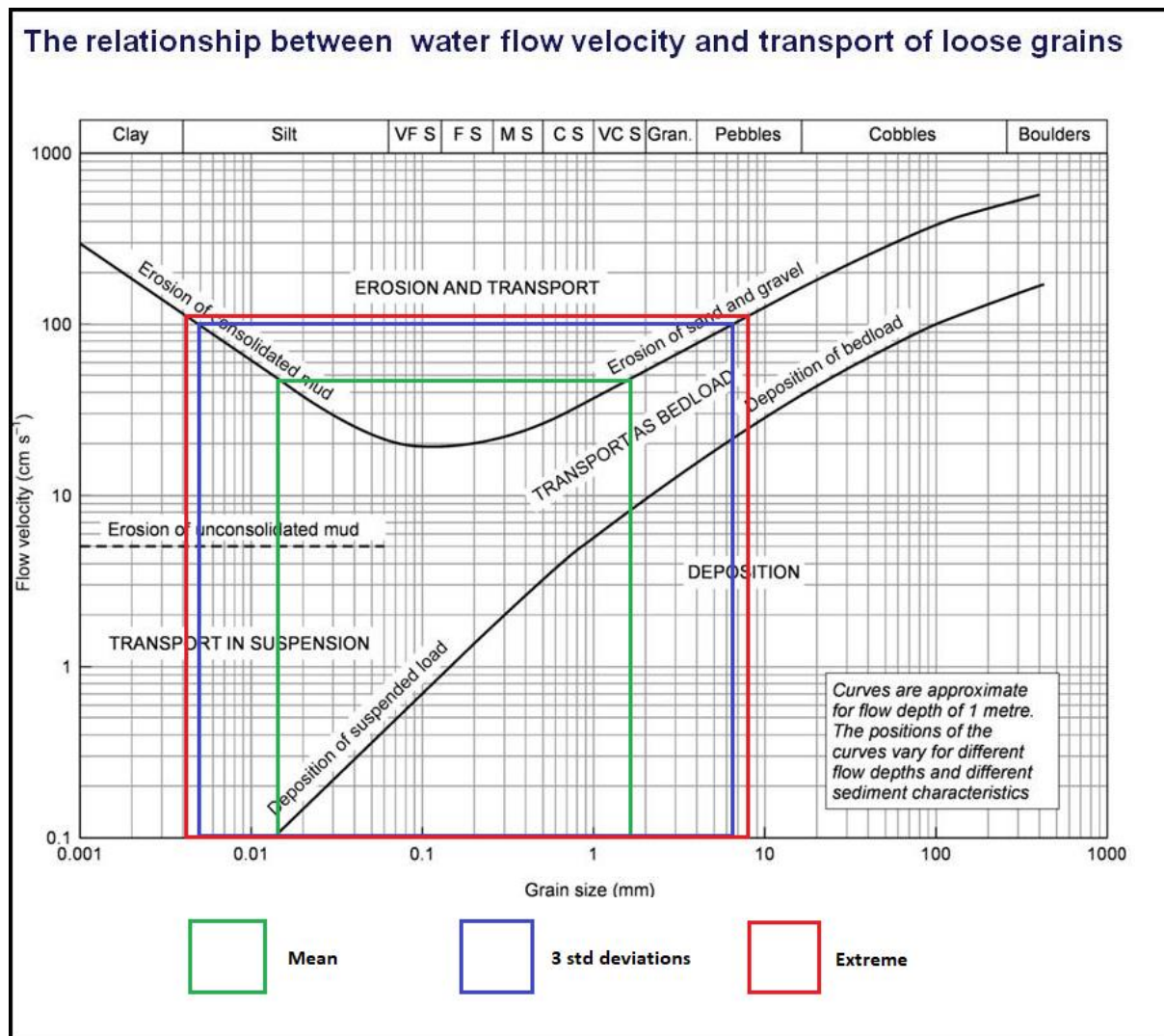
Figure 17: Hjulström Diagram, the green, blue and red boxes illustrating the NB current regime as listed in Table 7, figure by Gary Nichols 1999[35] and Vattenfall 2018.

Given the mean current-velocity of ~0.5 m/s (Table 7), erosion of medium grained silt – coarse sand is expected to be possible at most times, with erosion and transportation of fine-grained silt – small pebbles being possible 0.3% of the time. Extreme conditions will allow for some medium sized pebbles to mobilise.

Corelating the current properties and the lithological seabed classification (Figure 14) to the Bedform Stability Diagram illustrated by Figure 18, suggests the formation of ripples and subaqueous dunes to be the predominant features on the NB Site.
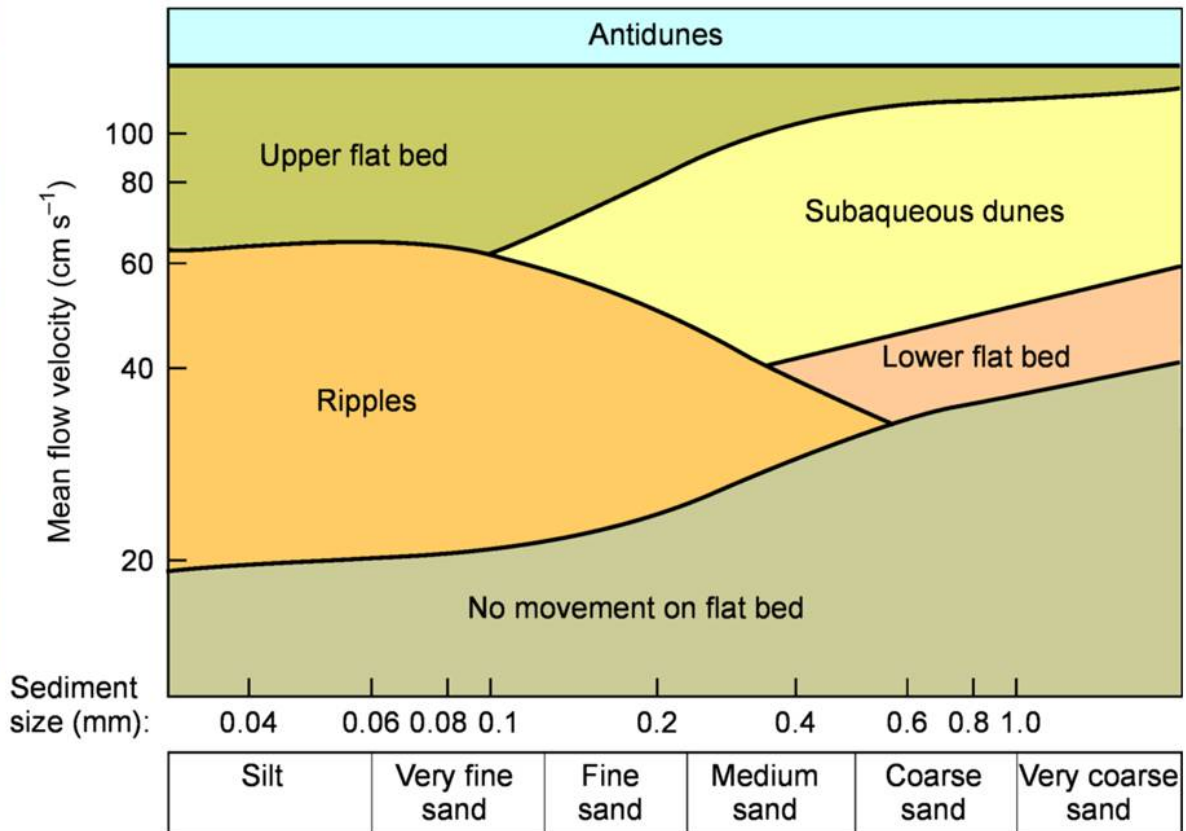
Figure 18: Bedform stability diagram, Nichols 2009[35].

In summary, the hydrodynamic conditions present on this Site are very well capable of eroding and transporting unconsolidated siliciclastic material, i.e. sands. Further, it is to be expected that tall sand-waves may develop given the significant tidal oscillation[21,33].

6. Bathymetrical Data

This section provides a more detailed investigation of the bathymetrical datasets used for the NB seabed model.

6.1. Bathymetrical data specifications

Several bathymetric datasets have been recorded at the site, with some only having insignificant coverage[5] which is insufficient for modelling purposes. The datasets included in this study due to their coverage, tie of acquisition and data quality are:

- Gardline 2010, EAOW[49,50]
- Fugro 2017[51]

6.1.1. Gardline 2010

Gardline Geosurvey Limited was contracted by East Anglia Offshore Wind Ltd to conduct an overview-survey throughout the East Anglia Development Zone. All coordinates quoted by Gardline were in WGS84 UTM31N, hence a conversion to ETRS89 UTM31N was undertaken for this report using Oasis Montaj 9.3. Specifications for the MBES data are:

- The positioning system is better than ±0.1m for 68% of time (1σ) and better than ±0.15m for 95% of the time (2σ).
- Regular Sound Velocity Profiles (SVPs) to be obtained.
- Simrad EM710/Simrad EM3002D multi beam echo sounders.
- GRS80 height reduced to LAT using the VORF[52] model.

Data were collected and processed to IHO Order 1 specifications[50,53].

Considering the water depth, data coverage, equipment spread and acquisition method used, the effective TVU will be ± 0.50 m (2σ) at 20 m water depth[53].The coverage of the 2010 survey is shown in Figure 19.The quality of the Gardline 2010 survey is considered sufficient for further analysis.

6.1.2. Fugro 2017

Data were acquired according to Vattenfall specification[54]. Data were requested to be acquired with an absolute accuracy (vertically and horizontally) of +/- 0,20 meter at 2σ (95% confidence level) and a data density of minimum 9 sounding per square meter with a 10% or higher swathe-overlap. The following specifications were attained:

- The positioning system was better than ±0.04m for 95% of time (2σ).
- Regular Sound Velocity Profiles (SVPs) have been obtained using a Valeport Sound Velocity Profiler.
- Kongsberg EM 2040 DualHead MBES.

The horizontal datum for the Fugro 2017 survey is ETRS89, UTM Zone 31 North. The vertical reference system for the Fugro 2017 data is LAT (VORF), derived from the GRS1980 Spheroid. The coverage of the 2017 Fugro survey can be seen in Figure 20. The quality of the data is considered sufficient for further analysis.

6.2. Data coverage

The data coverage of the surveys utilised for this report is illustrated in Figure 19, and Figure 20 on the following pages.

Several southeast-northwest oriented regional bathymetric highs are present over the site. They all display similar longitudinal orientation (south-southeast to north-northwest), coinciding with the predominant currents in the area, as described in section 4.

The width of the bathymetric highs varies from under 750m to more than 5km in the northern part of the site. The water-depth varies from -14m to -42m LAT. The highs have previously been classified as tidal ridges[2], which suggests they are oriented parallel to the dominant tidal currents (section 5). Sand-waves mostly strike perpendicular to tidal currents[17,20], and hence migrate along the tidal ridge-crests. The crests observed amongst the km-scale bathymetric highs in the area rise roughly between 2 and 10 m above the respective lows between them.
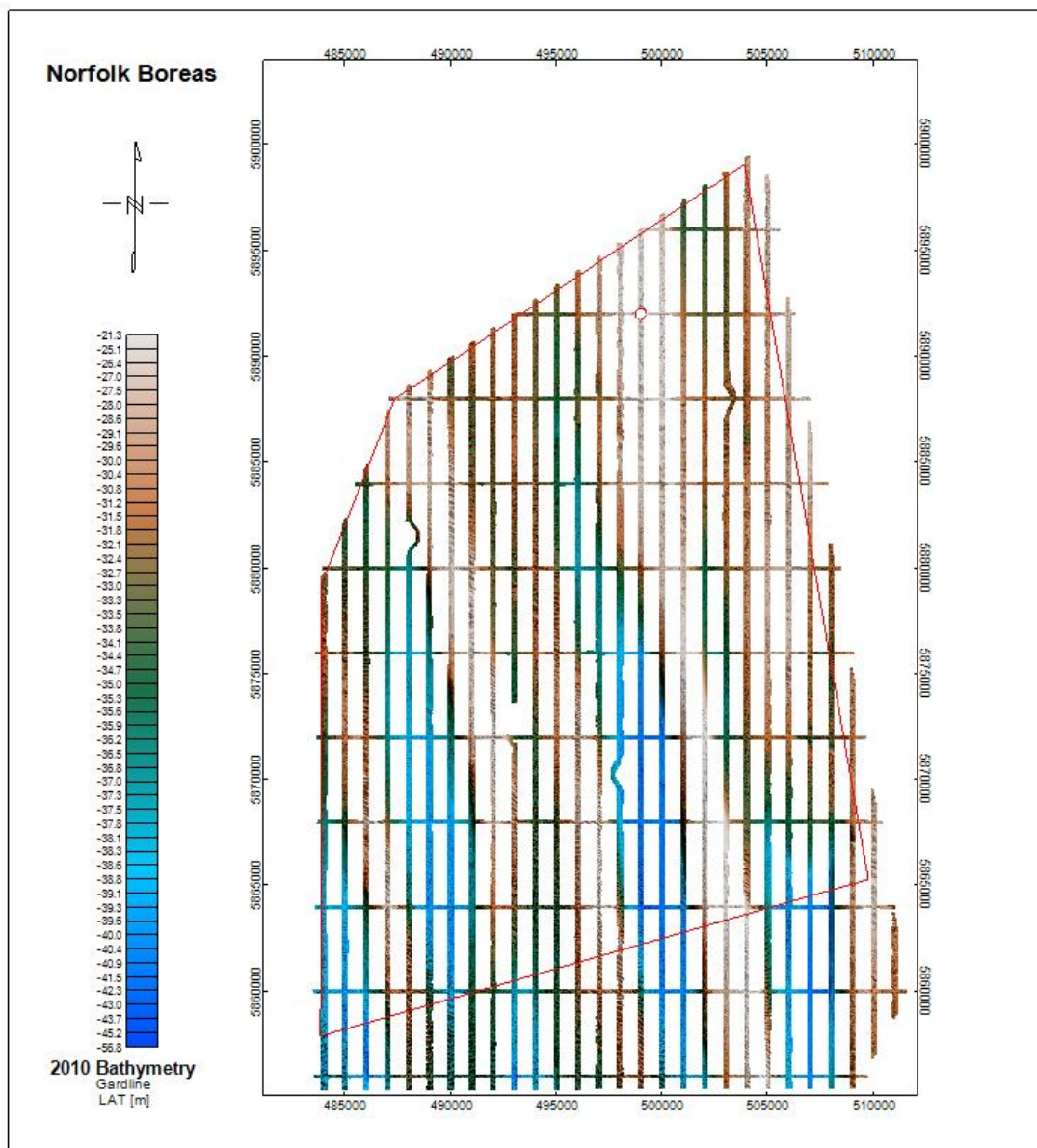

Figure 19: Gardline 2010 Bathymetry. The red outline encloses the NB site.

The water depth on-site generally lies in the range of -21 to -42 m relative to VORF LAT.
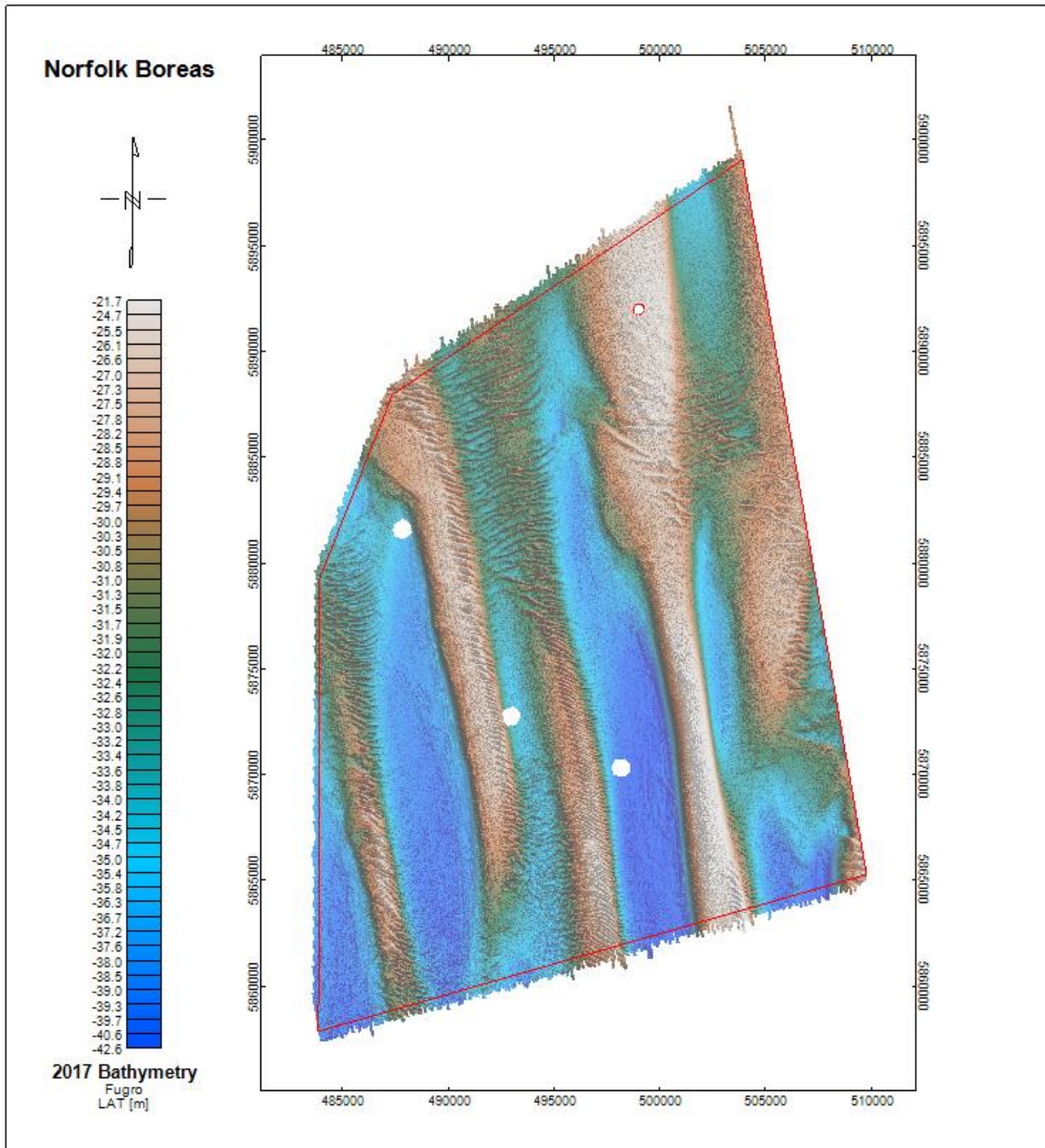

Figure 20: Fugro 2017 Bathymetry. The red outline encloses the NB site.

6.3. Naming convention of seabed structures

The naming convention used for this report is based on the Deltares[18] study. The relationship between scale and name is summarised in Table 8, and correlates the risk for construction of offshore structures in Figure 21. As tidal ridges (sand banks Figure 21) behave differently than sand-waves[2,21,35], and are generally considered stationary over the projected life-span of a wind-farm (25 years)[18], thus, they will be approached separately.

Feature name	Period of features	Vertical difference top to bottom
Ripples	20-30m	0 – 0.3 m
Mega-ripples	Ca. 30-100 m	0.3 – 1 m
Sand waves	100 m to 1 km	1 – 10 m
Sandbank	> 1 km	> 10 m

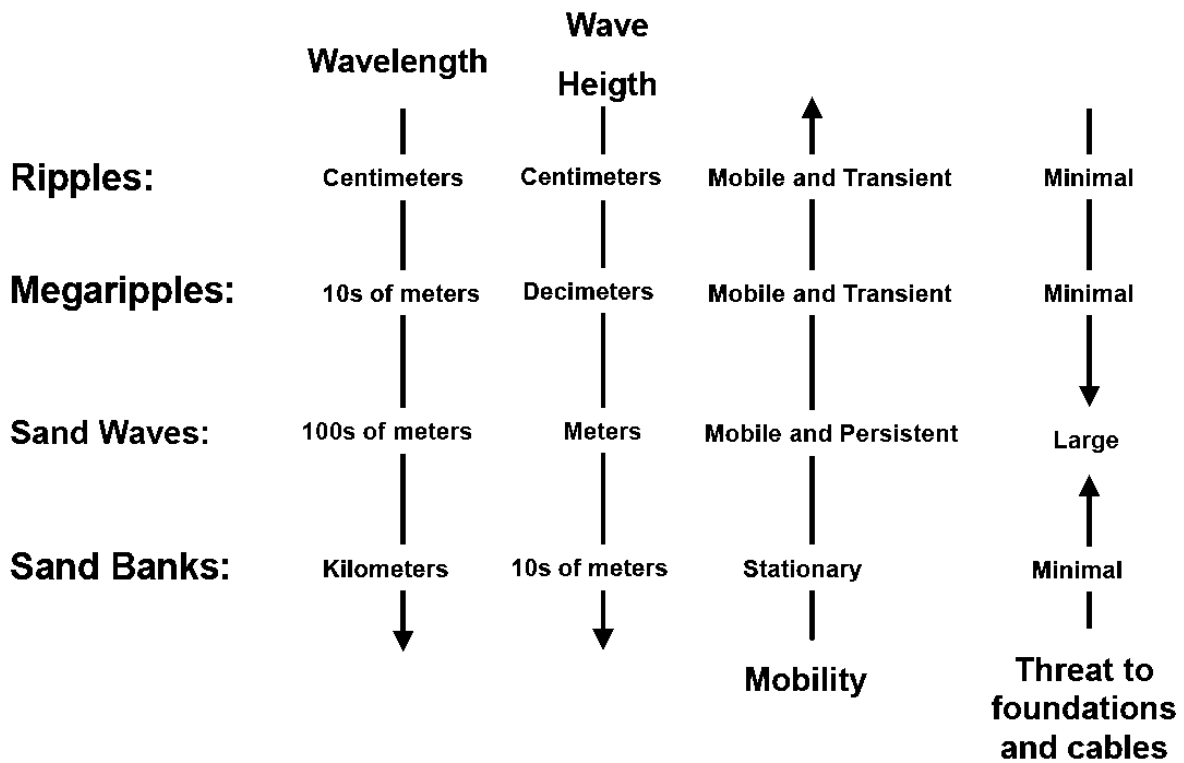Table 8 Overview of naming convention for this report

Figure 21: Seabed feature risk matrix provided by Deltares[18].

As illustrated by Figure 21, it is crucial to understand the behavioural properties of sand-waves to mitigate any structurally compromising loss of support-levels[12,18]. In section 7 of this report mobile features, with an emphasis on sand-waves will be isolated and described in detail.

Norfolk Boreas - Geophysical Seabed mobility assessment
Morphodynamic study   **Confidentiality class: High (C3)**
32 (72)

7. Norfolk Boreas Bathymetry

7.1. Observed differences in bathymetry data 2010 to 2017

To quantify any temporal change in bathymetry, the change must be measurable vertically and laterally. A quick assessment will be done in section 7.1.1 through a vertical difference grid, assessing the lowering and / or heightening of the seabed between 2010 (Gardline survey) and 2017 (Fugro survey).

7.1.1. Difference Grid

To assess actual seabed changes the bathymetry between 2010 and 2017 the 2017 z-component is subtracted from the 2010 z-component. The result is a 5-meter cell-size grid which is named *difference grid*, Figure 22.

The difference grid represents the vertical seabed changes over a period of 7 years. A statistical breakdown is illustrated by Table 9.

Table 9: Statistical breakdown of the difference grid.

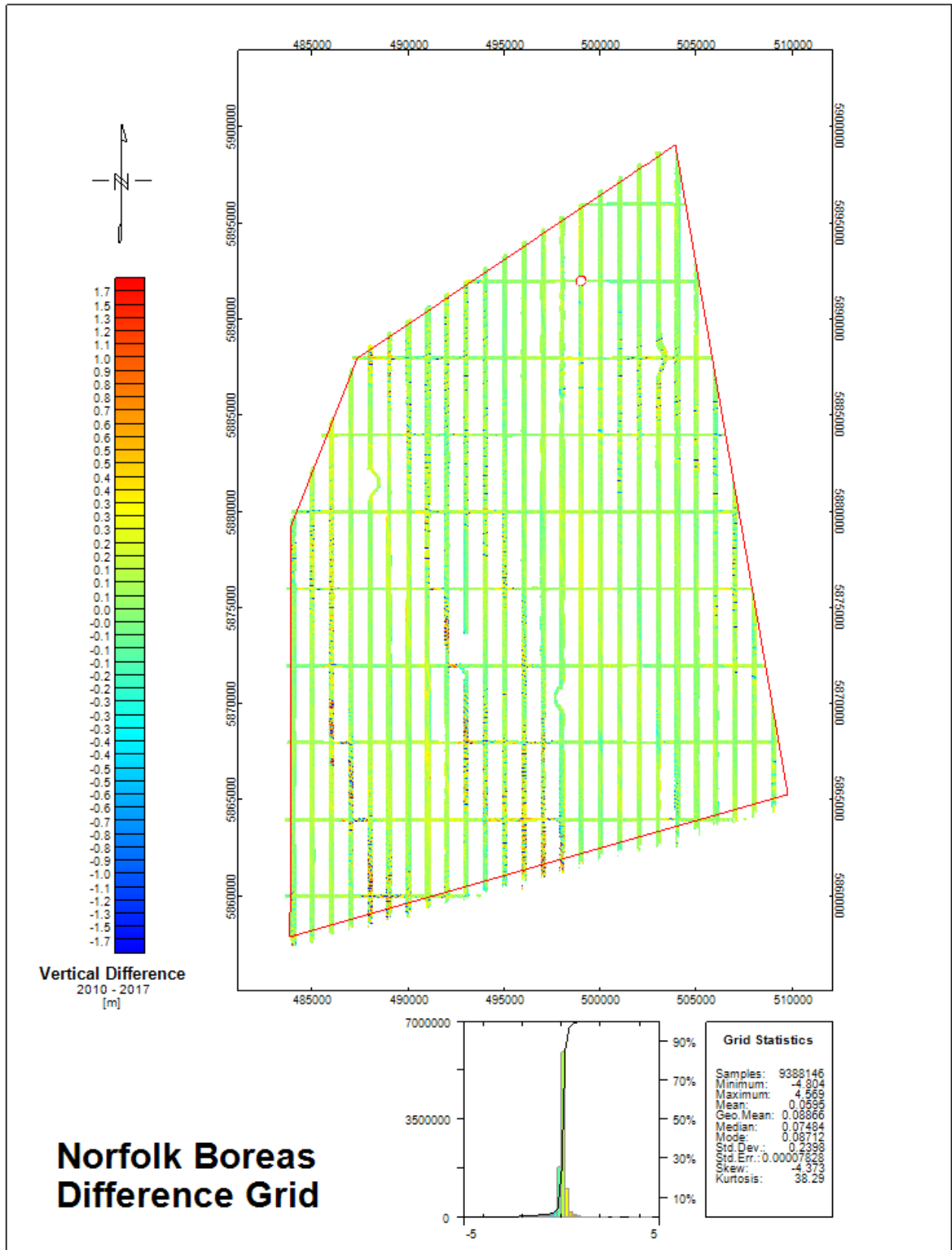| Parameter	Value [m]
Mean (average)	0.0595
Maximum sedimentation	4.569
Maximum erosion	-4.80
Standard Deviation, σ	0.24
Total Numbers, N	9388146

Figure 22: Difference grid, 2010 - 2017 vertical difference in metres.

Using the numbers extracted from the difference grid statistics, Table 9, it becomes evident from the width of the confidence-intervals (Table 10) for vertical change, that more targeted approach is necessary to produce valid assumptions for individual WTG positions.

Table 10: Interval of change considering the entire Site.

std.devs	Interval of change [m]	Percentage of data in the interval
1 σ	[-0.18, 0.30]	68.2689 %
2 σ	[-0.42, 0.54]	95.4499 %
3 σ	[-0.66, 0.78]	99.7300 %
4 σ	[-0.90, 1.02]	99.9936 %
5 σ	[-1.14, 1.26]	99.9999 %

Whilst a 5σ confidence level will comprise most of the site in terms of areal inclusion, the datasets are only offset by 7 years, which would suggest the confidence-intervals (Table 10) to be too narrow to comprise a potential life-cycle of the windfarm (25 years).

To assess this, the morphodynamic features need to be approached with a difference level of analysis, i.e. through a narrower lens, and hence, understood in greater detail.

7.2. Cross Sections & movement rates

A total of 27 cross sections have been made to investigate the movement of bedforms present on site. Cross sections are labelled A – Ø, their position and orientations are illustrated by the black lines in Figure 23. The cross sections are aligned with the Gardline 2010 survey corridors (Figure 19).
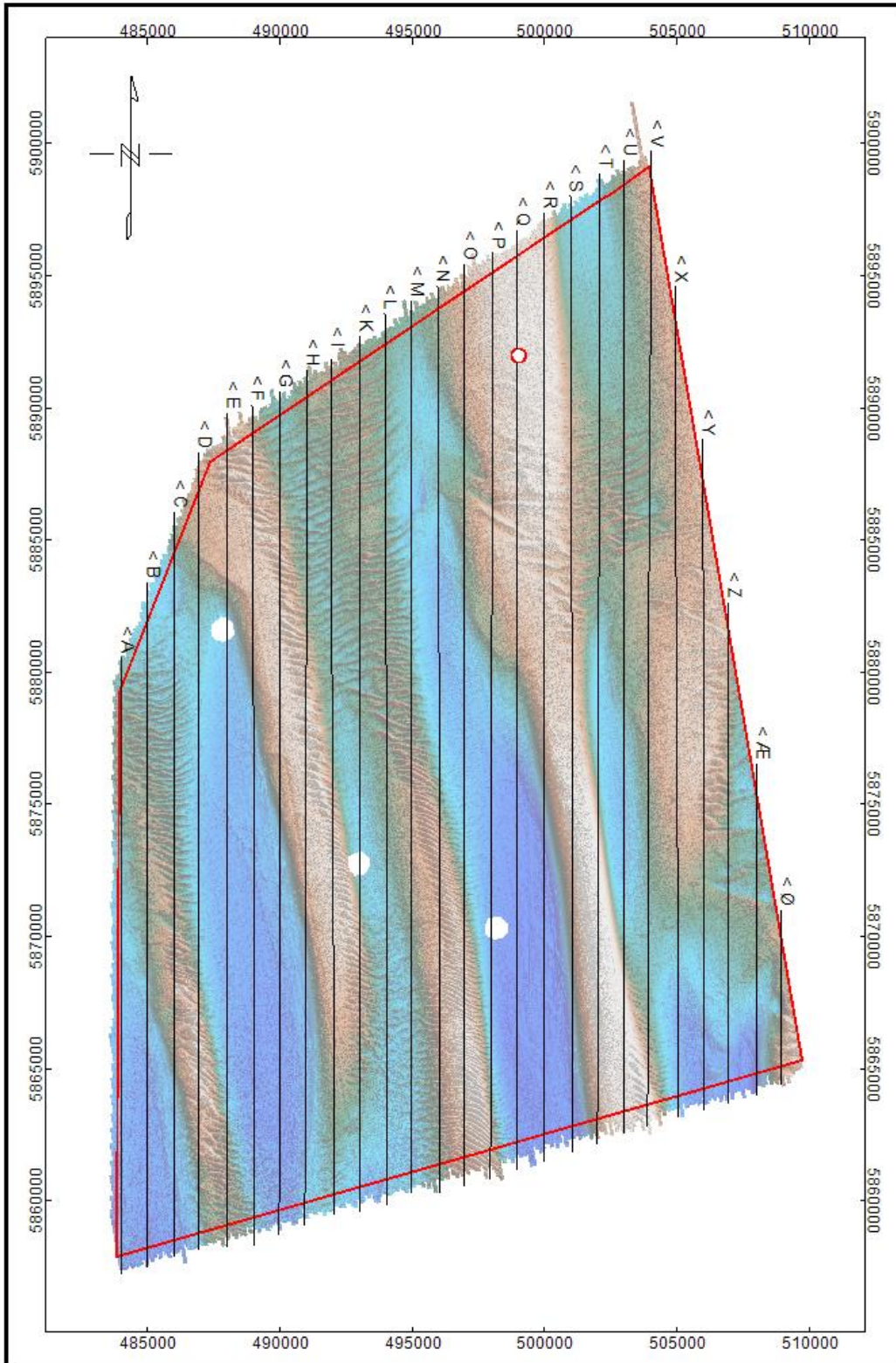

Figure 23: 2017 Fugro Bathymetry overlain by black lines representing cross section locations, arrow-heads indicate the sampling direction (South to North).

The profiles show bedforms (mega-ripples & sand-waves) migrating from South to North. Wave crests has been mapped using the 2017 datasets. Their (2017) lee-side slope locations (exceeding 4.5 degrees) are illustrated in Figure 24.
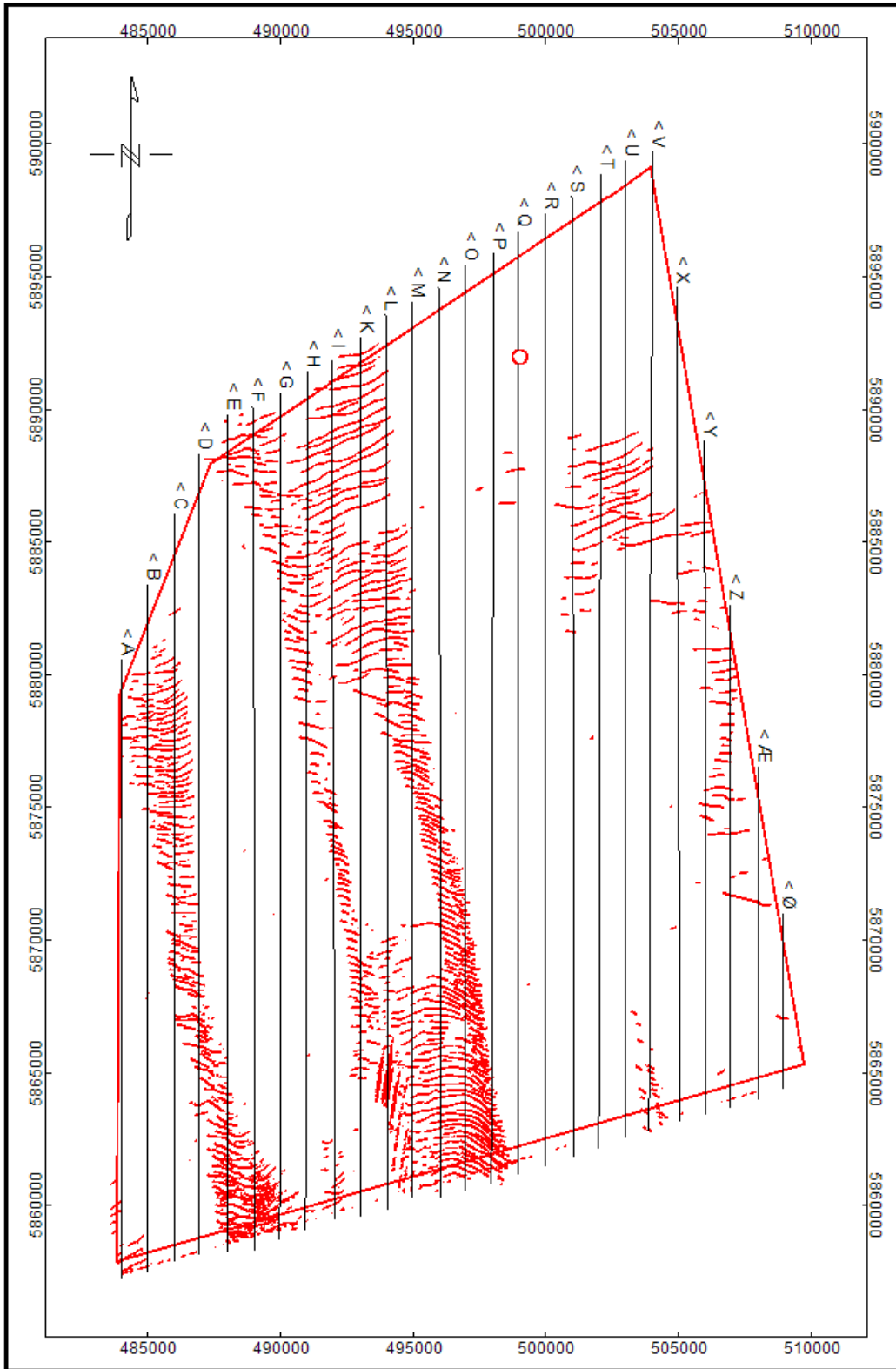

Figure 24: Slope magnitudes exceeding 4.5 degrees based on the 2017 bathymetry.

Figure 25 (below) shows the seabed through the northernmost part of section K. The section illustrates the lateral displacement of several sand-waves with wavelengths between 200 and 500m.
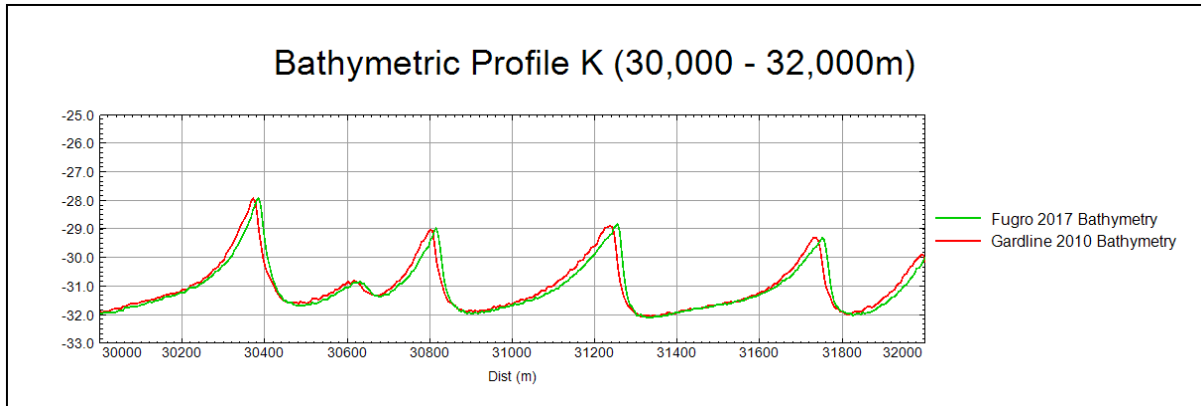

Figure 25: South - North Profile F crop. Horizontal and vertical scale in meters.

Similarly, structures with comparable dimensions have been identified with zero – little lateral displacement, illustrated in Figure 26 (below).
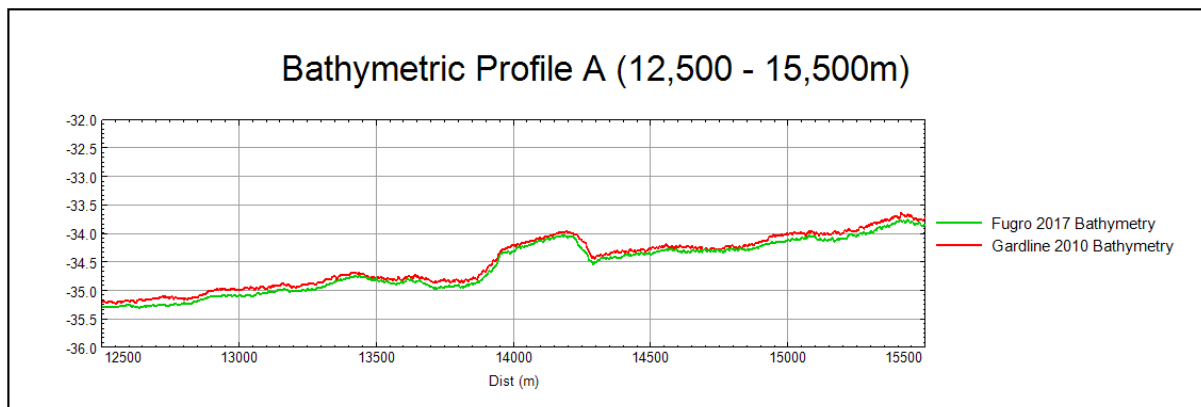

Figure 26: South - North Profile A crop. Horizontal and vertical scale in meters.

To accommodate these geometrically similar features the apparent velocity v of all bedforms was created. Each sampled point through all cross sections (A – Ø) was assessed in terms of South-North lateral offset between 2010 and 2017.

A cropped section of the bathymetric profile L is illustrated in Figure 27, to illustrate where the crest displacement was measured for the purpose of assessing the apparent velocity v. For sections with no quantifiable displacement, i.e. lateral offset < 1m between bedforms displacement was assumed to be 0.

No measurements were attempted for mega-ripples-displacements, as their rate of movement[1,48] and degradation[37] exceeds the sampling frequency (7-year period) available for this analysis.
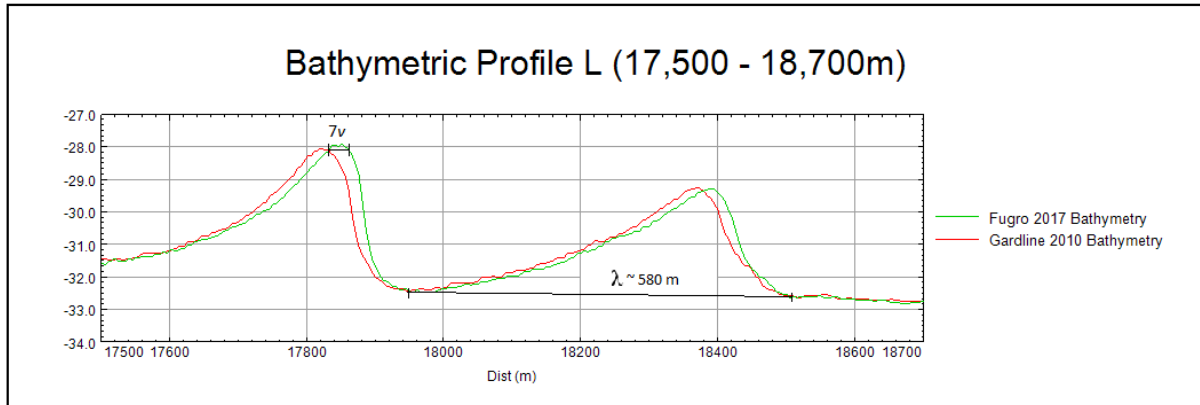
Figure 27: Point of measurement for the 7-year displacement, horizontal and vertical scales in [m].

These measured displacements are directly associated with their respective positioning in the Montaj database used for this purpose, an example of this sampling is demonstrated by Table 11, (*7v* in the database named is "*Displacement*").

✔ BOREAS_B:0	X	Y	G_2010_LAT_5m_A	G_Fugro_Boreas_2017_LAT_5m	Displacement
4303.0	484993.5	5879010.1	-31.8	-31.8	12.00
4304.0	484993.5	5879015.1	-32.7	-31.7	12.00
4305.0	484993.5	5879020.1	-33.1	-31.7	12.00
4306.0	484993.5	5879025.1	-33.3	-32.3	12.00
4307.0	484993.5	5879030.1	-33.5	-32.9	12.00
4308.0	484993.5	5879035.1	-33.7	-33.3	12.00
4309.0	484993.5	5879040.1	-33.7	-33.6	12.00
4310.0	484993.5	5879045.1	-33.8	-33.8	12.00
4311.0	484993.5	5879050.1	-33.8	-33.9	12.00
4312.0	484993.5	5879055.1	-33.8	-33.9	12.00
4313.0	484993.5	5879060.1	-33.9	-33.9	12.00
4314.0	484993.5	5879065.1	-33.9	-34.0	12.00
4315.0	484993.5	5879070.1	-33.9	-33.9	12.00
4316.0	484993.5	5879075.1	-33.9	-33.9	12.00

Table 11: Displacement sampling, Oasis Montaj database screenshot.

As these lines only present discrete values, it is assumed that a gradual relationship between displacement values exists, allowing for them to be gridded using the *Minimum Curvature* gridding algorithm. This algorithm will iterate through data points and provide the smoothest possible surface with 99% of point-data with 1% or less offset (absolute values) from the resulting grid[55]. Gridding will begin at $8 \cdot 125m$, and with no point being offset more than 50% of the line-spacing from a data-point each cell will comprise 1 or more actual data-points, hence, an area-wide distribution of displacement values is established.

The result of these gridding iterations is a smoothed grid with a 125m cell-size, comprising the apparent south – north displacement of seabed structures through the 2010 – 2017 period. This grid had all cell-values divided by a factor of 7 to produce the apparent annual displacement velocity *v* [*m/y*].

The result of the gridding is illustrated in Figure 28. The grid correlates with the hypothesis, described in section 3, of tidal furrows between the sand-ridges being void of mobile content with only little displacement recorded outside of sand-wave fields.
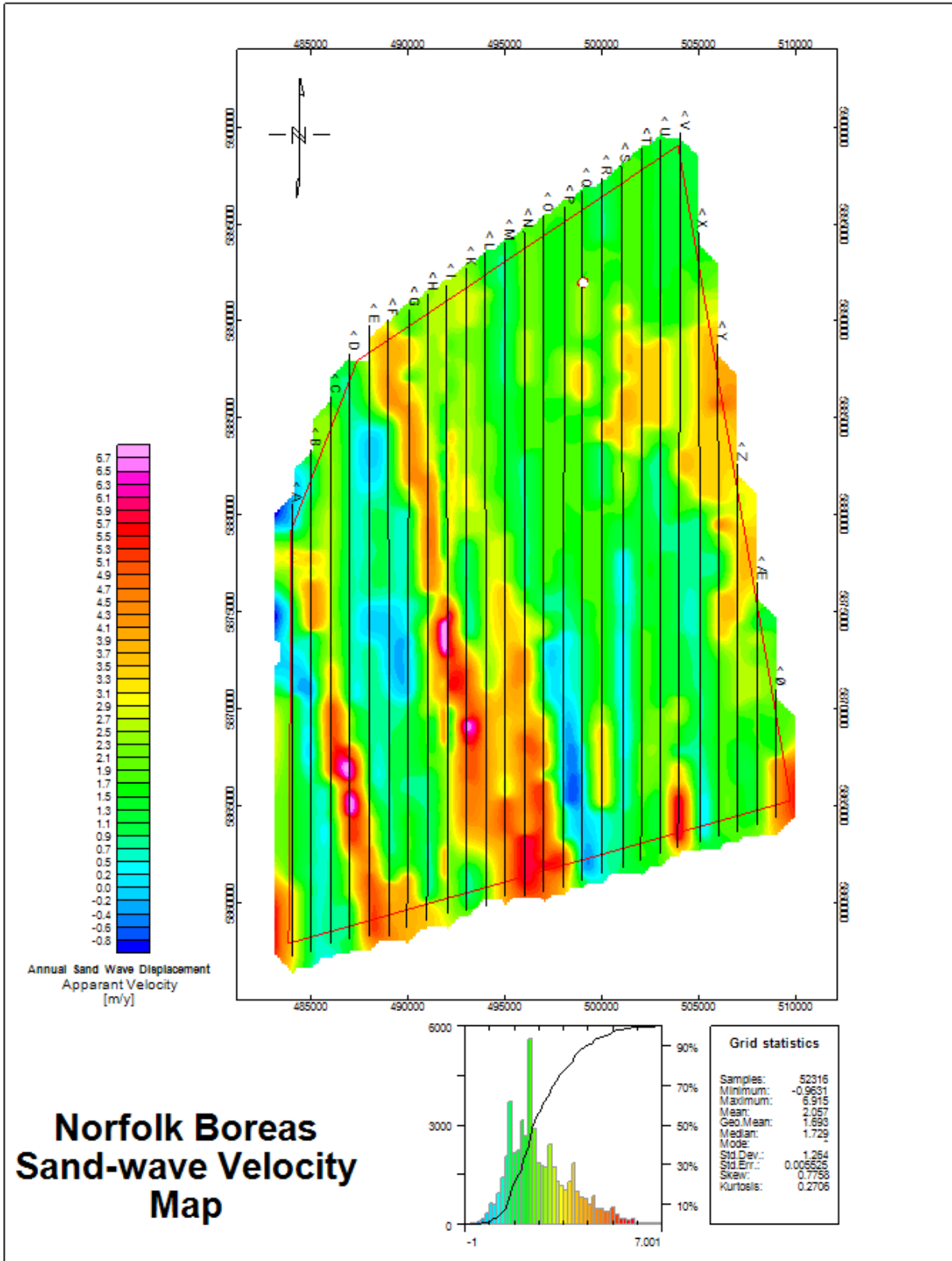
Figure 28: Apparent displacement velocity grid. Black lines showing the cross sections used for sampling.

As the measured offsets are oriented south-north, this will not directly reflect the actual northwards migration of sand-waves. The migration is mainly perpendicular to the lee-side of the sand-wave, which aligns with the residual tidal current-direction $\pm 10°$ [2,8,16,18,20,34,35].

The lee-slope is often very steep, in excess of 15 degrees[35], which allows for them to be mapped based on their gradient magnitude in Oasis Montaj. Illustrated by the red line-features in Figure 29.
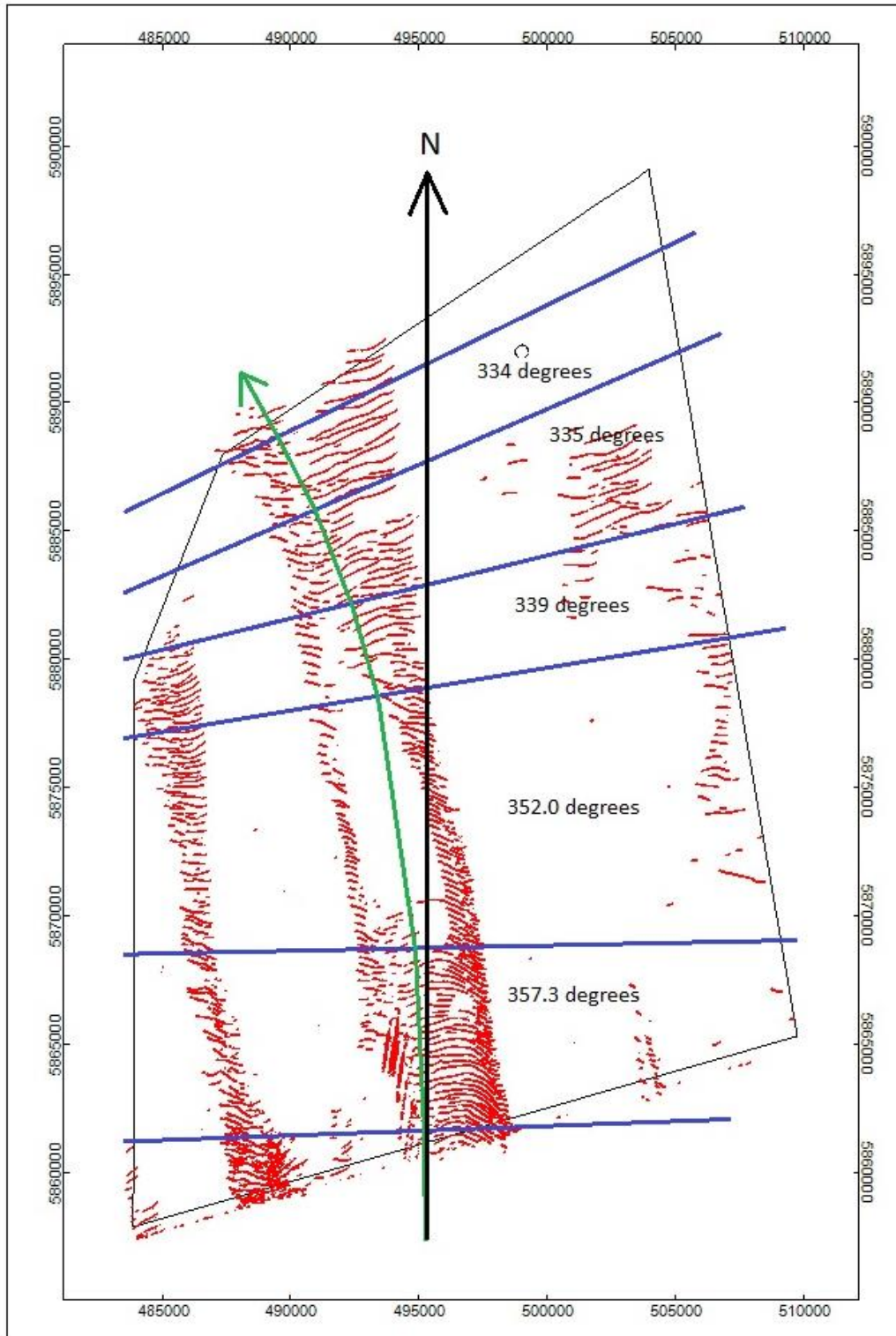

Figure 29: Slopes exceeding 4.0 degrees. Based on the 2017 bathymetry (5m dtm) with interpreted orientation of lee-side slope-strike (red lines) and movement direction of bedforms (green arrows).

Following this approach, the best-estimate movement direction was assessed to be

$a = 334 - 357 \degree$ NNW. Knowing the northbound apparent velocity (v) and the direction, the annual displacement of a point (x, y) was isolated. As the apparent velocity was factored in as $v = \langle dx, dy \rangle = 1$, the concept is illustrated by Figure 30.
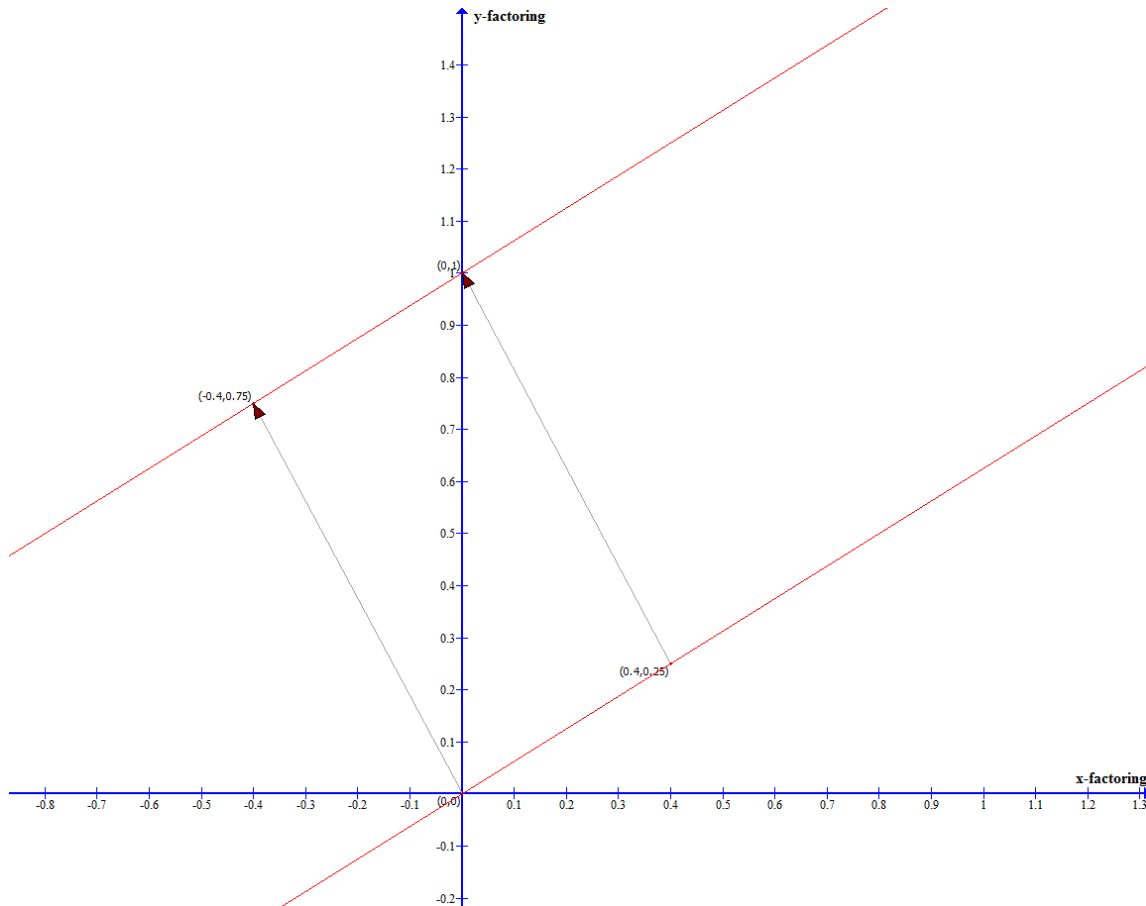

Figure 30: Discrete point-displacement based on the apparent velocity (illustrative example).

The $\langle dx, dy \rangle$ components have thus been reduced to

$$dx = sin(360\degree - a) \cdot v$$
$$dy = \cos(360\degree - a) \cdot v$$

This is incorporated into the Montaj database when calculating the annual change to be

$$X_n = X_0 - (n(v \cdot dx))$$
$$Y_n = Y_0 + (n(v \cdot dy))$$

With n being the time in years from the initial year (2017), X and Y being the coordinates of a given point in the year $n_0 = 2017$.

As mega-ripples could not be modelled in terms of annual movement-rates and directions based on the available data, they are considered a noise-constraint for this models' precision. In order to accommodate this noise, any bedform shorter than 50m was isolated for statistical quantification. Results are shown by Figure 31.
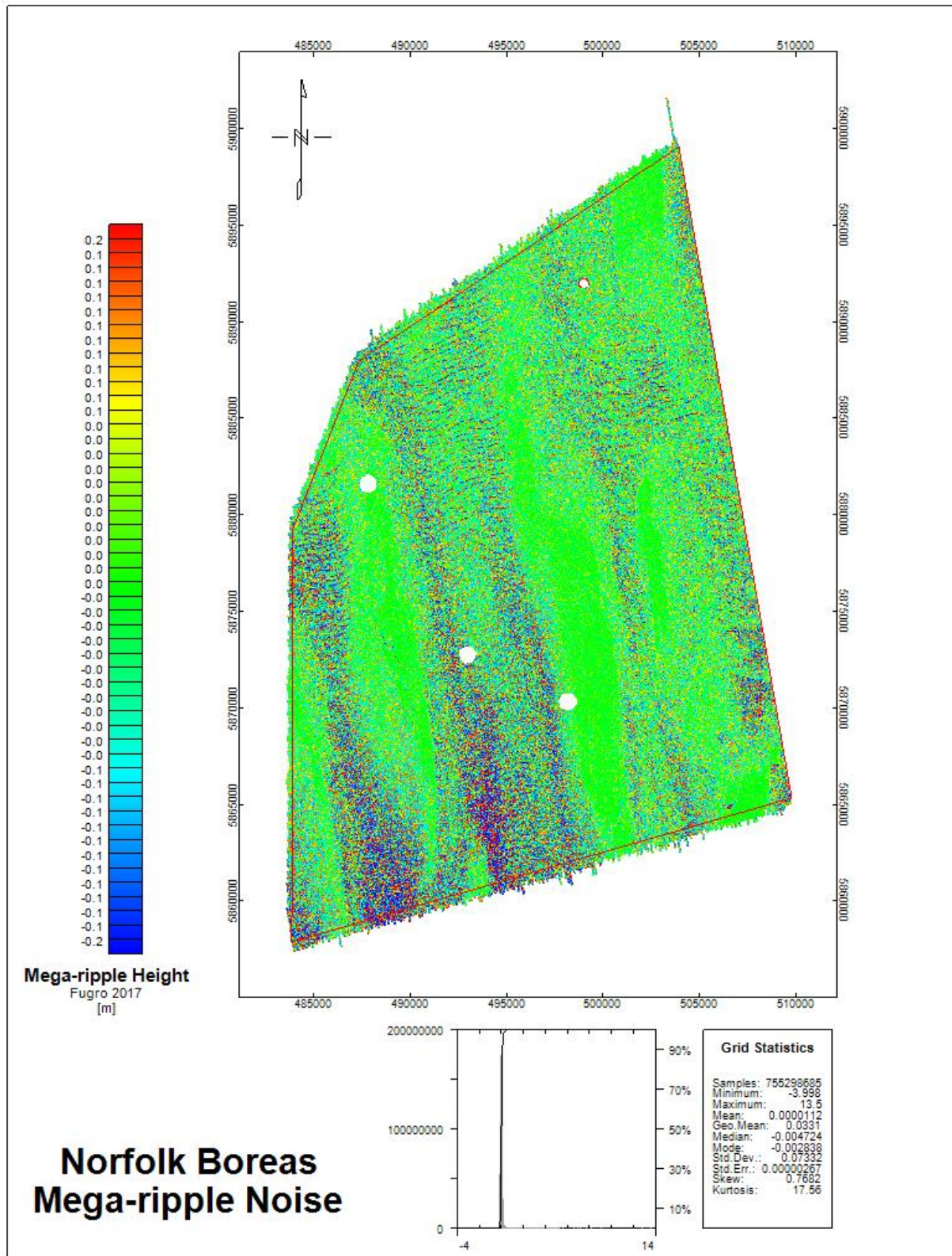
Figure 31: Short bedforms with no resolved displacement measurements.

The smoothed surface was modelled by gridding the 2017 Fugro bathymetry mean levels using a 12.5m cell-size, which will ignore wavelengths shorter than 50m corresponding to the

Nyquist-theorem. Bedforms were isolated by subtracting the 1m bathymetry model from the 12.5m cell-size mean-value bathymetry grid.

The effect of this can be illustrated in a cross section (Figure 32). Overall the noise-levels might be slightly optimistic and a 3σ confidence interval (99.7%) is chosen over the regular 2σ (95%) confidence level, to account for a reasonable level of uncertainty.
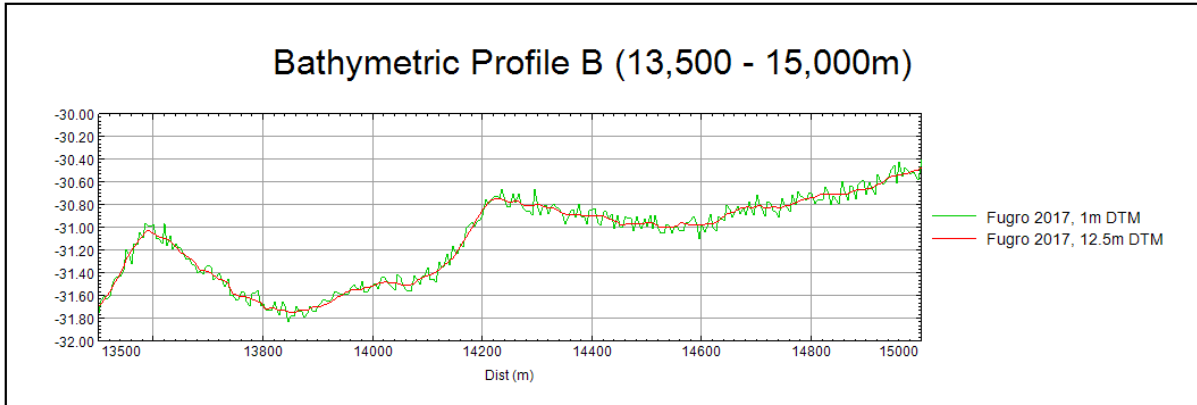

Figure 32: Filtering of short bedforms.

Given the noise level (3σ) of $\pm0.220m$, and adding to this the vertical MBES uncertainty of the 2017 described in section 6 of $\pm0.20m$ a total vertical model uncertainty (*TVU*) of $\pm0.42m$ must be expected.

Thus, it must be presumed that the *Best Estimate* (Mean) must be nested within the bounds of a *Highest Seabed Level* (Mean + *TVU*) and a Lowest Seabed Level (Mean – *TVU*).

Upper (HSBL), lower (LSBL), and Best Estimate (BE) model surfaces were created for the timespan between 2020 and 2055 as per Table 12.

Table 12: Derived seabed models.

Year	Best Estimate	Lowest Seabed Level (LSBL)	Highest Seabed Level (HSBL)
2020	√	√	√
2025	√	√	√
2030	√	√	√
2035	√	√	√
2040	√	√	√
2045	√	√	√
2050	√	√	√
2055	√	√	√

To transpose the sand-waves according to the $\langle dx, dy \rangle$ components, they must be isolated from the overall bathymetry, which is achieved through a minimum level direct gridding algorithm, which allows for a cell to adopt the minimum value of a highly oversampled dataset (9 points per m^2) across a 200m grid-cell. The resulting grid will provide a smooth base level which converges with sand-wave troughs. This grid is smoothed further in a re-gridding process reducing cell-size to 25m to better mimic generic sediment behaviour.

This method assumes mobile sand-thickness to attenuate towards the base of the sand-wave troughs. Highly resolvable SBES times series (annual re-surveys 2000 – 2010, 2013 and 2017) have shown this to be true in the nearshore-regions of the Danish North Sea[32,56], as well as Deltares having this approach certified as best-practice in 2016[18] for the Dutch regions of North Sea, hence this assumption is carried forward.

A cross-section (K, Figure 33) illustrates the smoothed 200m minimum grid in green (sand-wave base level) situated under the 2016 1m bathymetry grid in red.
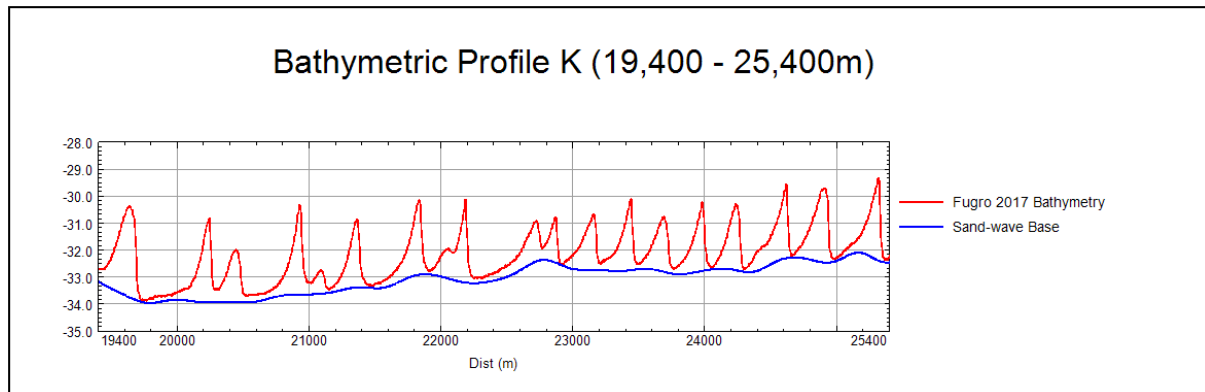

Figure 33: Cross section K, Fugro 2017 bathymetry overlaying the smoothed 200m minimum grid level. Horizontal and vertical scales in [m].

The overlying unit defines the *Mobile Bedform Layer* (MBL), which comprises the volume of sand-waves, mega ripples and other bedforms / outcrops with similar wavelengths. Through the application of the velocity components stable outcrops will not be moved and stay rooted at their original position.

The MBL can be quantified statistically, Table 13, which shows a wide range of bedform amplitudes ranging from few to some meters. The maximum value has been searched for and found to be a generically unrelated outlier.

Table 13: Statistical breakdown of the Mobile Bedform Layer

Parameter	Value [m]
Minimum	0.00
Maximum	8.58
Mean (Average)	0.73
Median	0.48
Standard deviation (σ)	0.67

The distribution of isolated bedforms is illustrated by Figure 34.

Figure 34: Mobile Bedform Layer (MBL) thickness. Isolated from the Fugro 2016 bathymetry.

Correlating the MBL to the previously shown gradient plot (Figure 24), indicates a high degree of correlation between the picked slopes and isolated bedforms, illustrated by Figure 35.
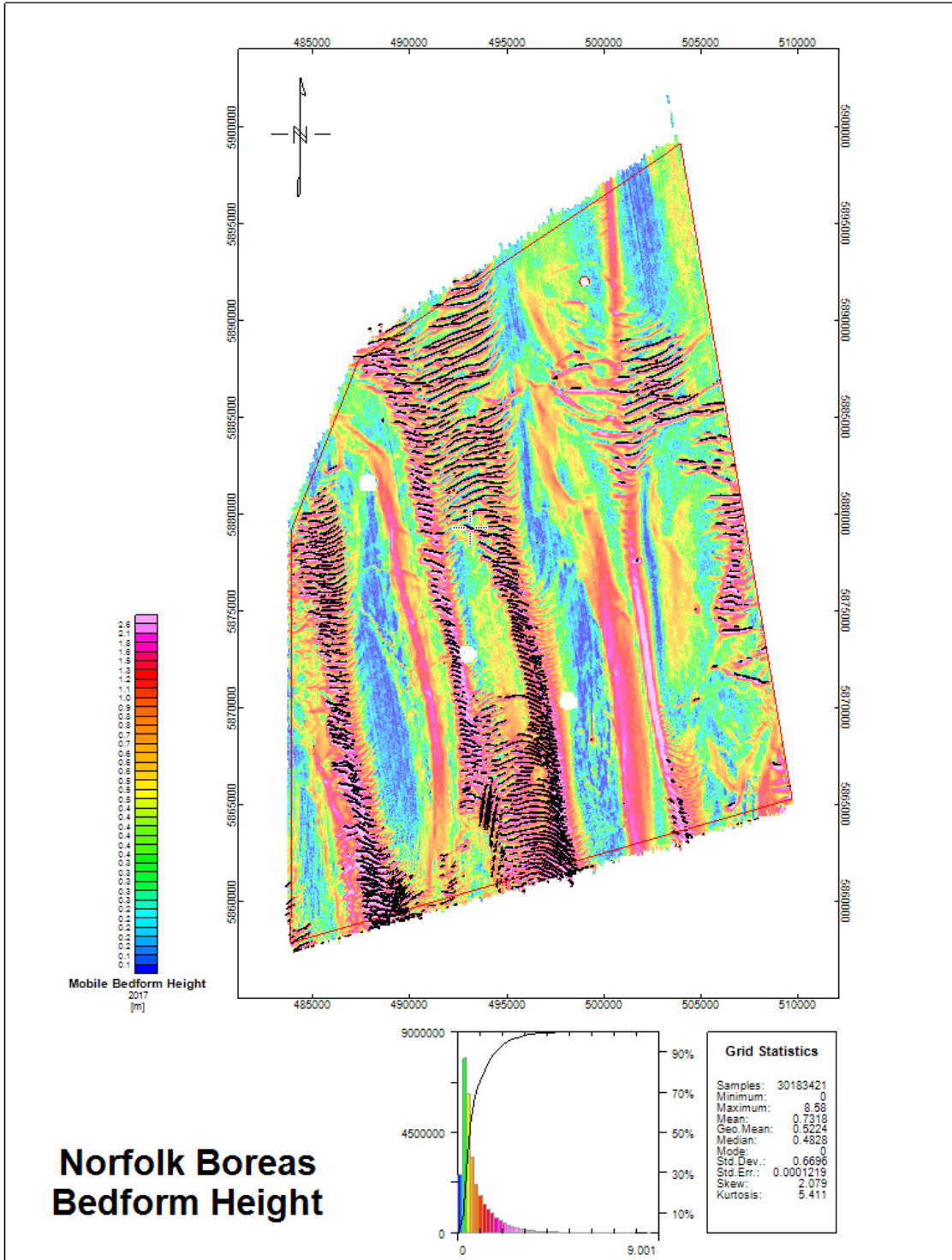
Figure 35: Mobile Base Layer (MBL) overlain by the picked lee-side slope magnitudes exceeding 4.5 degrees (black lines).

As described by Voepel et. al 2013[57] the residing time of all given grains will follow an approximate Pareto-distribution, implying the bulk of observed migration being the result of a continuous rework of the same material. Hence, suggesting the probability to be re-suspended, i.e. the probability to contribute to the formation of mobile bedforms, increases by the first suspension and so forth. This coincides with the observed pattern of clustered sand-waves.

7.3. Model properties

By applying the velocity variables $\langle dx, dy \rangle$ isolated in section 7.1 to the MBL and adding it to the residual seabed (RSB) a constructed seabed containing points *X and Y* for any given year (*n*) following (or preceding) 2017 can be constructed assuming X_{-n} and Y_{-n} are true.

An example from cross-section Q (location illustrated by Figure 23, oriented south to north) is illustrated by Figure 36. The models for 2025, 2035, …, 2055 were sampled. Surfaces were calculated in 5-year intervals, not all displayed in this figure.
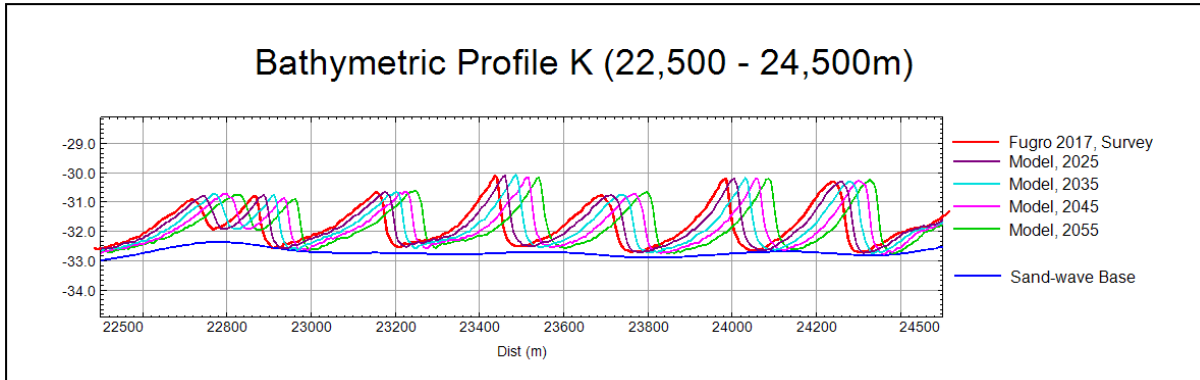

Figure 36: Cross-section K sampling the 2017 bathymetry and the modelled seabed for 2025, 2035, 2045 and 2055. Horizontal and vertical scales in [m]

To accommodate the model-uncertainty the LSBL and HSBL grids are calculated, starting in 2017 (*n = 0*) as the Bathymetry ± TVU, rounded up to 0.50 m, and following this as the lowest (for the LSBL) or highest (for the HSBL) value of any preceding or given surface through a true-false statement in Oasis Montaj, for instance the year-n LSBL.:

$$n\_LSBL = \text{Where } n\text{-}5\_LSBL <= n\_Model - TVU$$
$$\text{Then } n\text{-}5\_LSBL$$
$$\text{Else } n\_model - TVU;$$

Which in Montaj will be

$$G0 = (G1 <= G2\text{-}0.42) \ ? \ (G1) : (G2)$$

$$G0 = LSBL\_n$$
$$G1 = LSBL\_n\text{-}5$$
$$G2 = n\_model$$

This accounts for the expected erosion while neglecting any local replenishment by approaching bedforms, i.e. providing the lowest possible global seabed level in any point for a given year. This will over time lead to a visible erosion of the MBL and the modelled LSBL will converge with the Static-seabed-grid given enough time. In practice this is overly conservative on a global or even regional scale but provides a fair local lower-bound prediction.

Similarly, the HSBL is calculated by assuming no erosion while incorporating the gradual accumulation from approaching bedforms.

The upper and lower bounds will be gradually be more conservative, which is roughly illustrated by Figure 37, showing the trend towards higher general seabed lowering (LSBL) and heightening (HSBL).
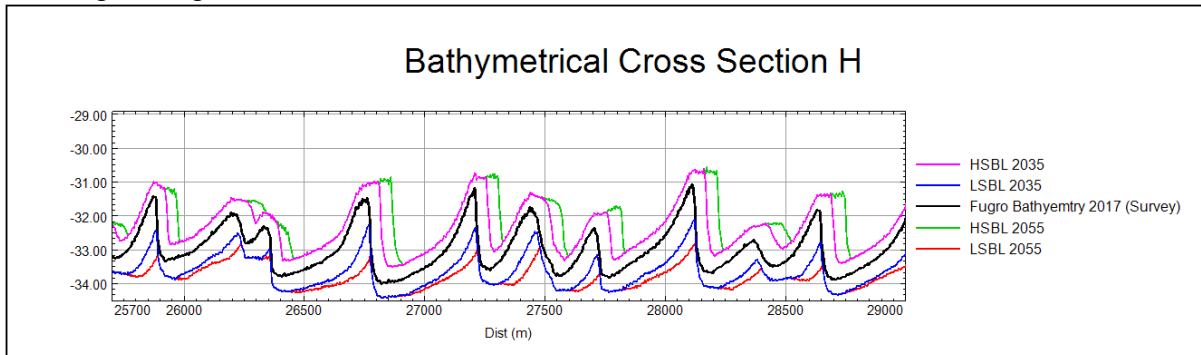

Figure 37: 2035 and 2055 LSBL & HSBL surfaces encapsulating the 2017 bathymetry. Horizontal and vertical scales in [m]

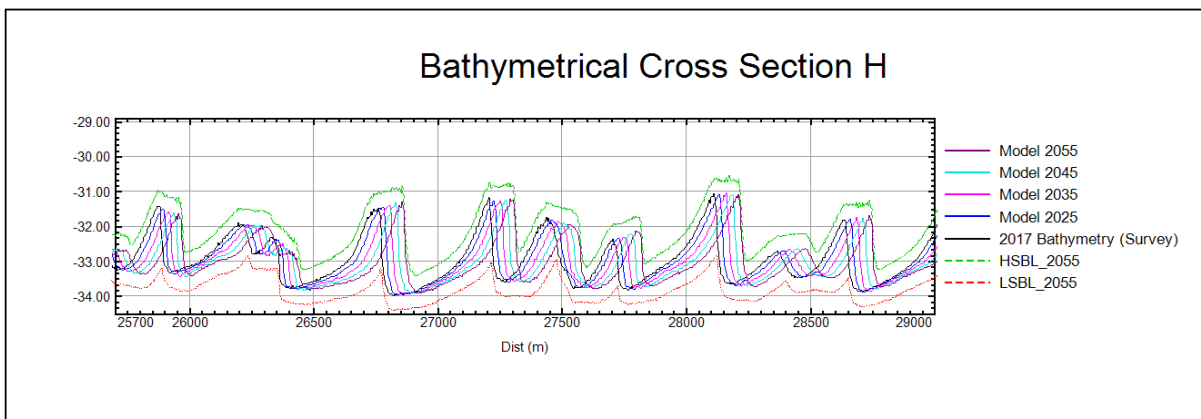A visualisation of the 2055 LSBL and HSBL is illustrated by Figure 38.

Figure 38: 2055 LSBL & HSBL encapsulating the 2017 - 2055 modelled bathymetry along part of cross section Q. Horizontal and vertical scales in [m]

As displayed in Figure 38, the upper and lower bound estimates should be considered the most conservative seabed-level estimate at any given point in time between 2016 and 2056.

A difference plot between the 2055 LSBL and HSBL grids has been produced to illustrate the potential vertical intensity of change throughout the site (Figure 39 and Figure 40).

Figure 39 shows the most extreme-lowering of the seabed between 2017 and 2055. This lowering exceeds the Best Estimate lowering by 0.42m.
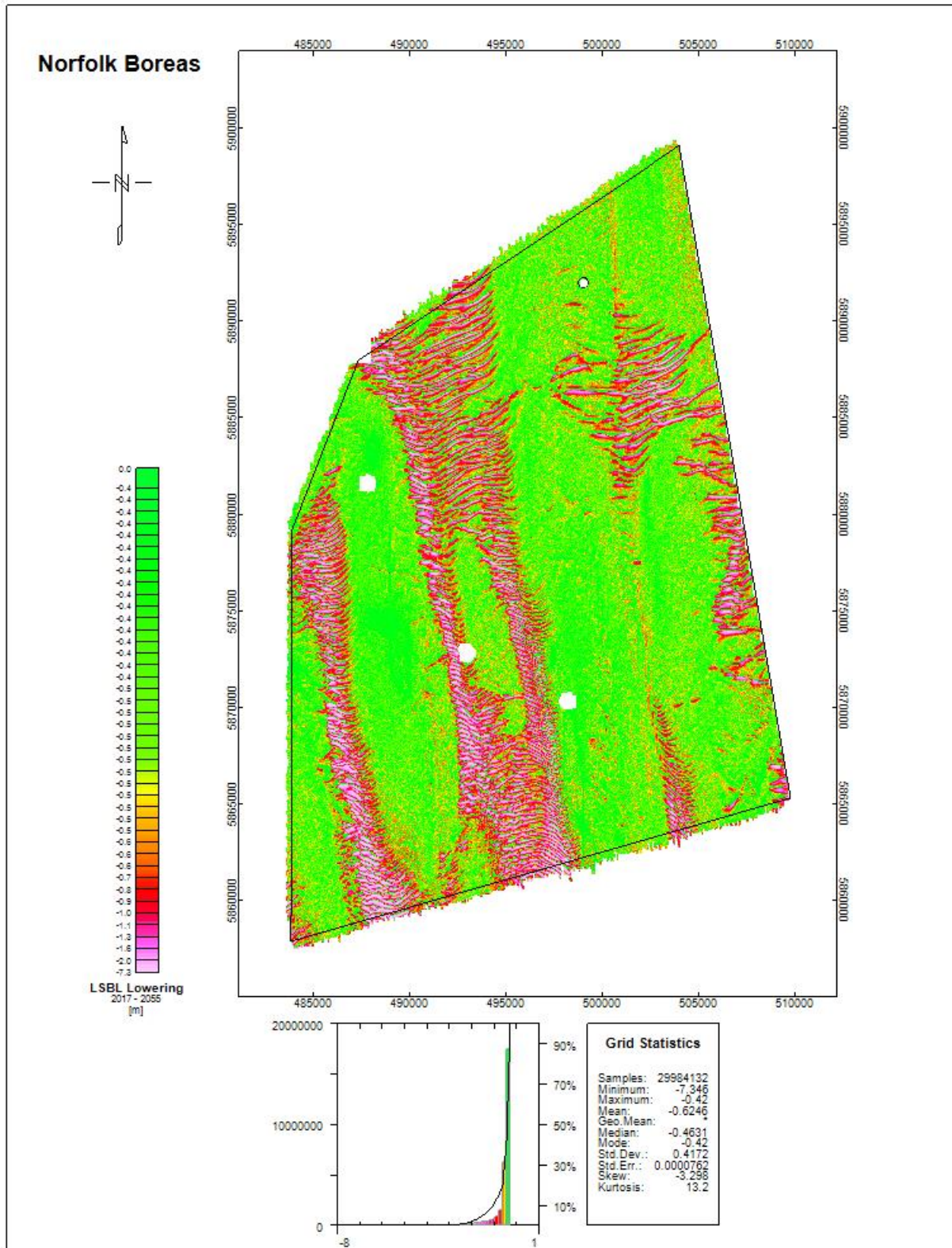

Figure 39: Difference between 2017 bathymetry and 2055 LSBL

Figure 40 shows the most extreme-heightening of the seabed between 2017 and 2055. This heightening esceeds the Best Estimate heightening by 0.42m.
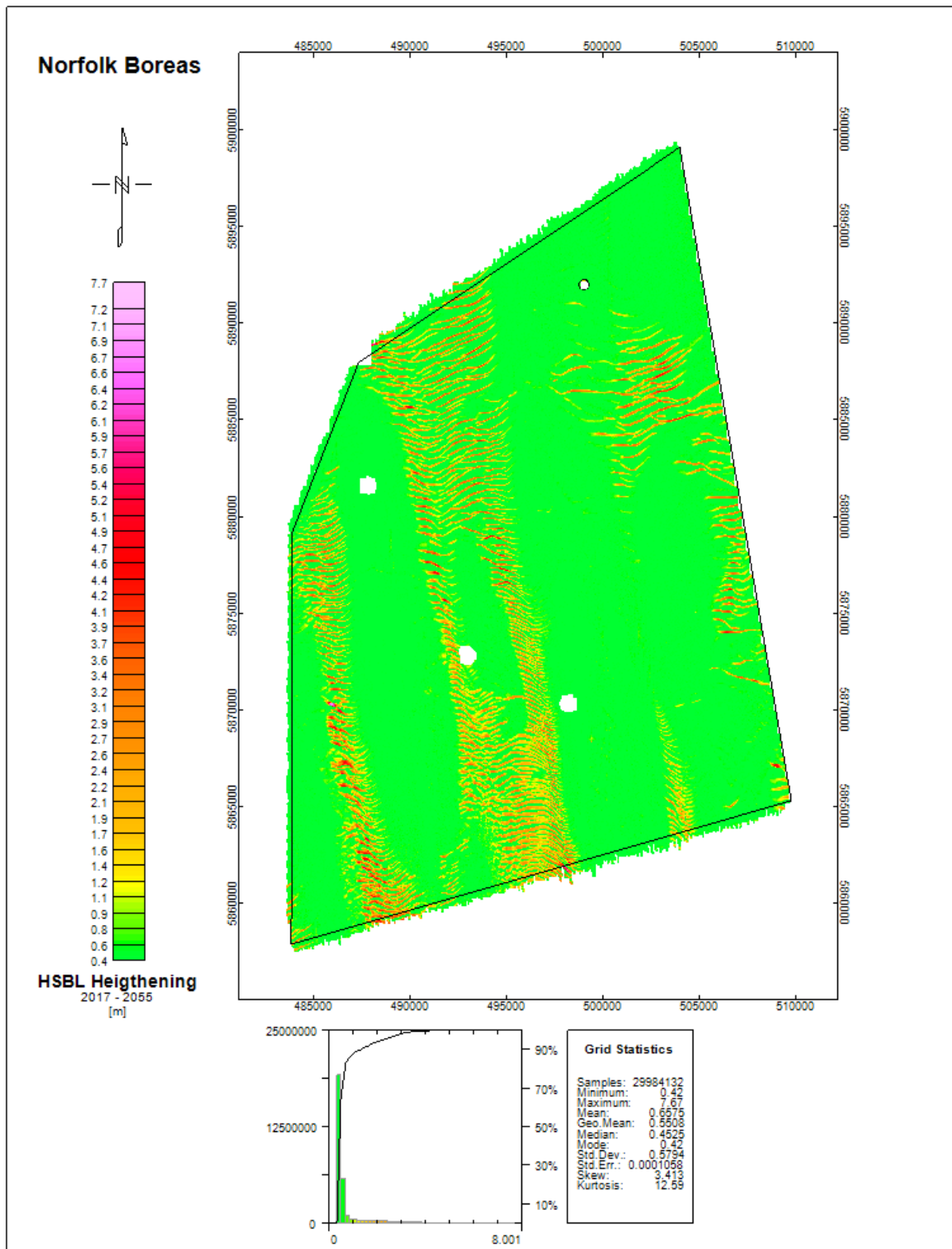

Figure 40: Difference between the 2017 bathymetry and 2055 HSBL.

7.4. Model Verification and Validation

As some uncertainties will always be present within a geological (or geophysical) model[58], the aspiration for any model is to reduce the number & magnitude of as many uncertainties as possible. To assess the precision and applicability of a given model, a model simulation can be compared to observations (survey data)[59].

As the model developed for NV-West was developed based on the 2016 Fugro MBES data, comparisons can be made with the Gardline 2010 MBES survey data. As the primary aim of the model is to predict sand-wave movements, the comparison will be focusing on validating an appropriate displacement of sand-waves.

In a cross-sectional view, Figure 41 and Figure 42 it is illustrated how the 2010-model mimics the 2010 bathymetries spatial distribution of sand-waves.
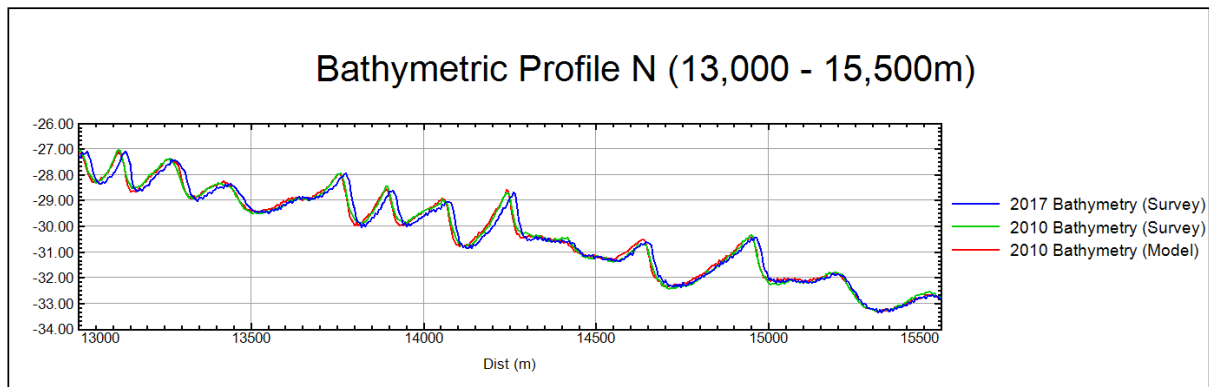

Figure 41: Cross section Q interval. Horizontal and vertical scales in [m]
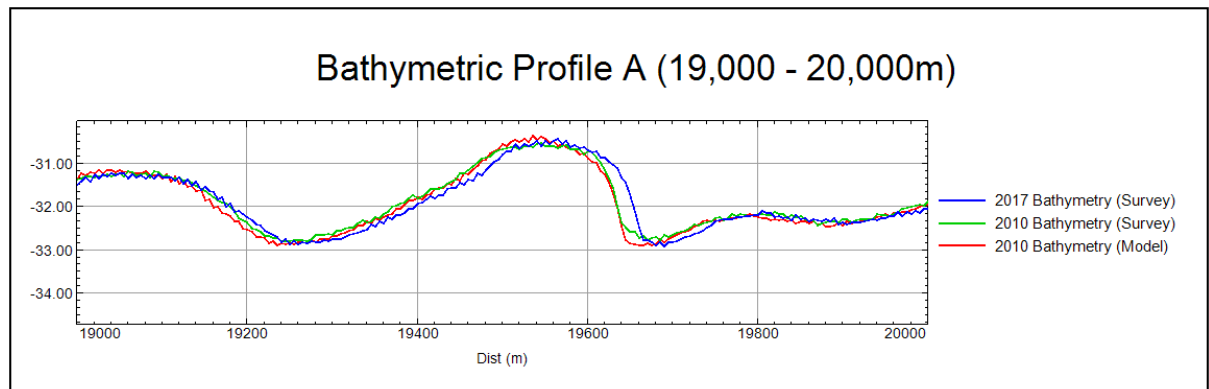
Figure 42: Cross Section O interval. Horizontal and vertical scales in [m]

Based on inspections performed on the 27 cross-sections (location shown by Figure 23) it is concluded that sand-wave displacement-offsets have been effectively attenuated through 3 iterations of the velocity model.

To test for vertical accuracy a difference grid between the 2010 Model and the 2017 Fugro bathymetry is calculated (like Figure 22). If the model is to be considered probable, the std. deviation from the mean should be within a narrow range of the one derived from Figure 22 and listed by Table 9.

The 2010 Model vs 2017 bathymetry difference grid is illustrated in Figure 43. The 5σ confidence interval for this grid is [-1.39, 1.39] which offsets the [-1.14, 1.26] confidence interval by less than the 2017 vertical MBES uncertainty (±0.20m) and the mega-ripple noise (±0.22m).
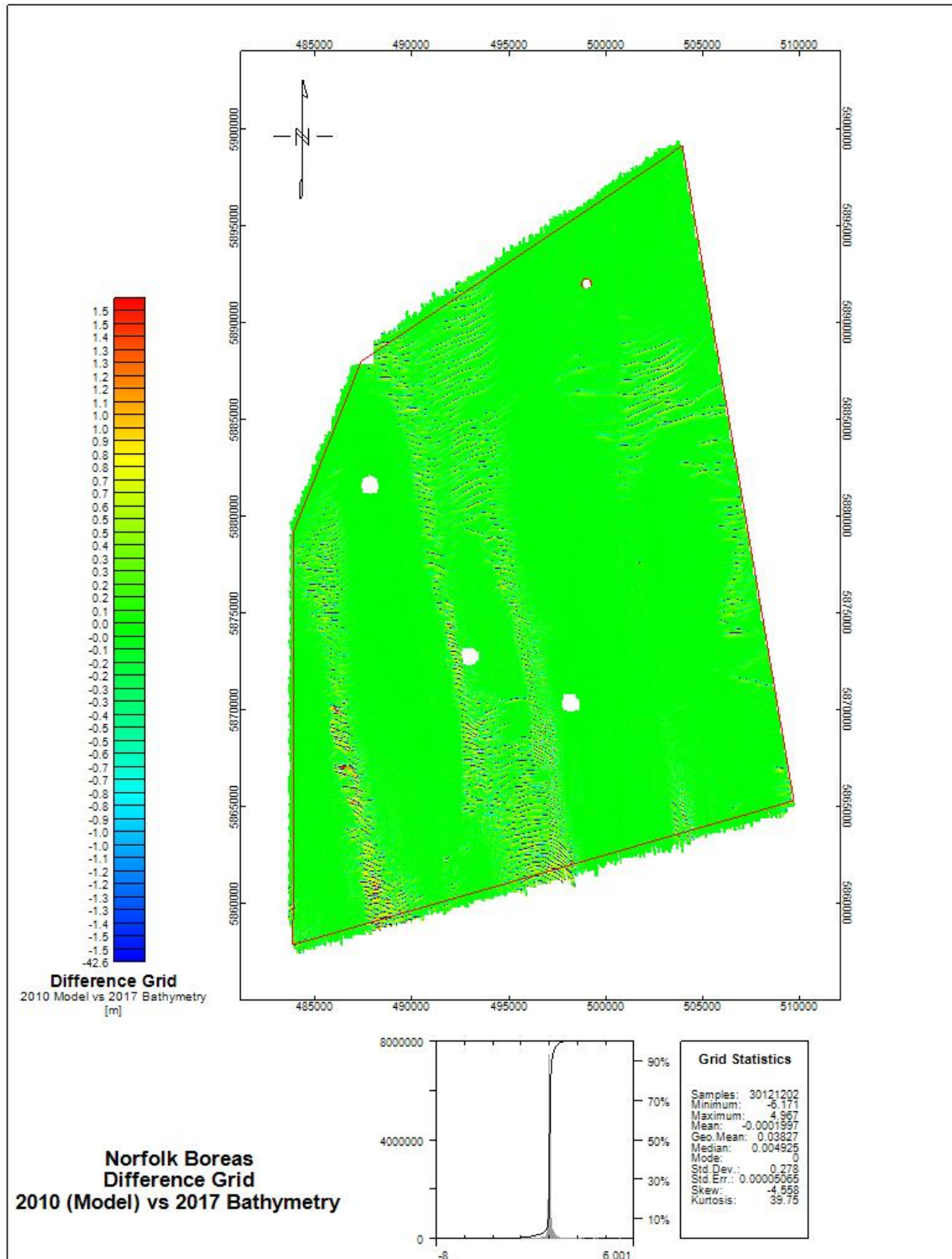
Figure 43: 2010 Model vs 2017 Bathymetry difference grid.

For a comparison between Figure 22 and Figure 43 see Table 14.

Table 14: Difference grid comparison.

Parameter	Value [m] (2010 Survey vs 2017 Survey)	Value [m] (2010 Model vs 2017 Survey)
Mean (average)	0.06	0.00
Maximum sedimentation	4.56	4.97
Maximum erosion	-4.80	-5.17
Standard Deviation, σ	0.24	0.28
Total Numbers, N	9388146	30121202

Based on the figures displayed in this section, it is determined that the established model is producing a vertical & lateral prediction-values resembling the empirical measurements acquired by Gardline in 2010[50].

7.5. Model application

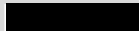Using the model described in section 6.7 of this report, a lower bound, best estimate, and upper bound prediction of the bathymetry for the years 2020, 2025, …, 2055 has been established. It is assumed that each model surface is valid for ± 2 years[60] for general guidance purposes. For installation of any structure it is recommended by the author of this report to re-survey the perimeter following the IHO special-order guidelines[53], as the model cannot predict non-linearities in sediment migration, deposition and other sudden extreme cases influencing the sediment succession[29].

The upper and lower prediction bands both include the 0.5m uncertainty band resulting from survey-uncertainties and the rapid migration of mega ripples. An example of the seabed prediction along a randomly selected cross section is shown in Figure 36.

The Best Estimate (BE)-, LSBL-, and HSBL-models were sampled for all layout scenarios shown in Table 15.

Table 15: Layouts investigated for this report.

Case	Layout
1	■■■■
2	■■■■
3	■■■■

This allows for a database comprising the Vattenfall Layout to sample each grid at the suggested WTG location. Following this sampling each subsequent value (2020 – 2055) was normalised compared to the 2017 bathymetry measured by Fugro, i.e.
[Surface] – [Reference Surface] = [Anticipated change], to produce a graphical illustration of the relative changes at each discrete location. For this, the reader is referred to the appendices.

The following values were evaluated (Table 16):

Table 16: Values evaluated for each WTG-layout.

Year	Best Estimate	Lowest Seabed Level (LSBL)	Highest Seabed Level (HSBL)
2020	√		
2025	√		
2030	√		
2035	√		
2040	√		
2045	√		
2050	√		
2055	√	√	√

Where [*NA*] is stated, the WTG position is not within the bounds of the given model-surface. For more comprehensive tables than those shown in Section 7.5.1 – 7.5.3 and for a graphical illustration of the prediction ranges in the years 2020 - 2055 the reader is referred to the appendices to this report.

It must be noted that some WTG positions are situated too close to the western / southern edge of the 2017 bathymetry grid to be included by the model.

7.5.1. ████████████████

A geographically referenced plot of ███████ is illustrated in Figure 44 and the predictions made for each WTG location are listed by Table 17.

Figure 44: OLNV0016 Layout plot on Fugro 2017 Bathymetry.

Table 17: Layout ▮▮▮▮▮▮ predictions for global seabed changes. Values in [m].

ETRS89 UTM31N		Turbine ID	Water depth (LAT [m])	Modelled Vertical Change [m]				
X	Y		Measured (2017)	2020	2025	2030	HSBL	LSBL

7.5.2. ▬▬▬▬▬ (Case 2)

A geographically referenced plot of ▬▬▬▬▬ is illustrated in Figure 45 and the predictions made for each WTG location are listed in Table 18.

Figure 45: OLNV0014 Layout plot on Fugro 2017 Bathymetry

Table 18: Layout ▓▓▓▓▓ predictions for global seabed changes. Values in [m].

| ETRS89 UTM31N | | Turbine ID | Water depth (LAT [m]) | Modelled Vertical Change [m] | | | | |
X	Y		Measured (2017)	2020	2025	2030	HSBL	LSBL
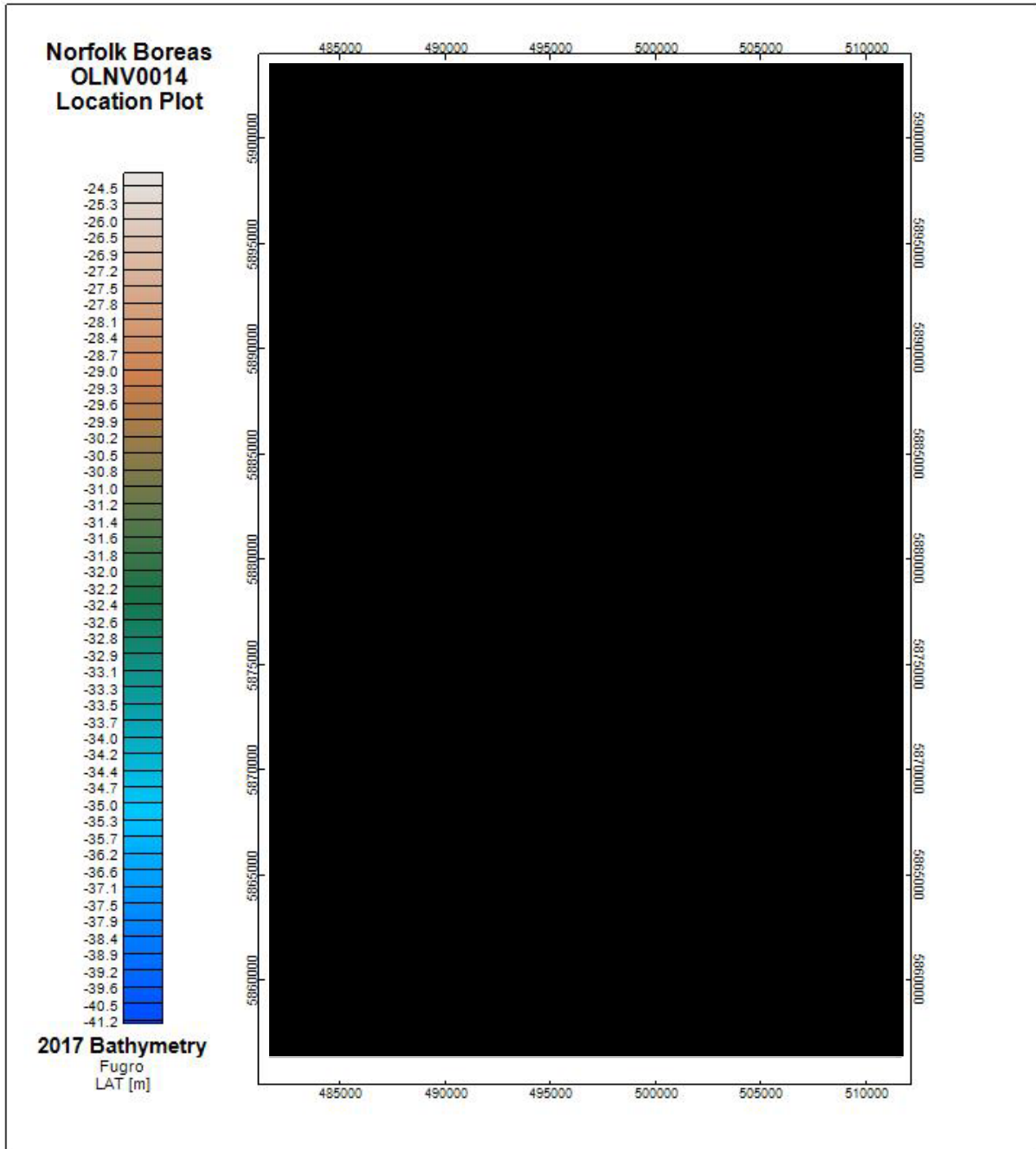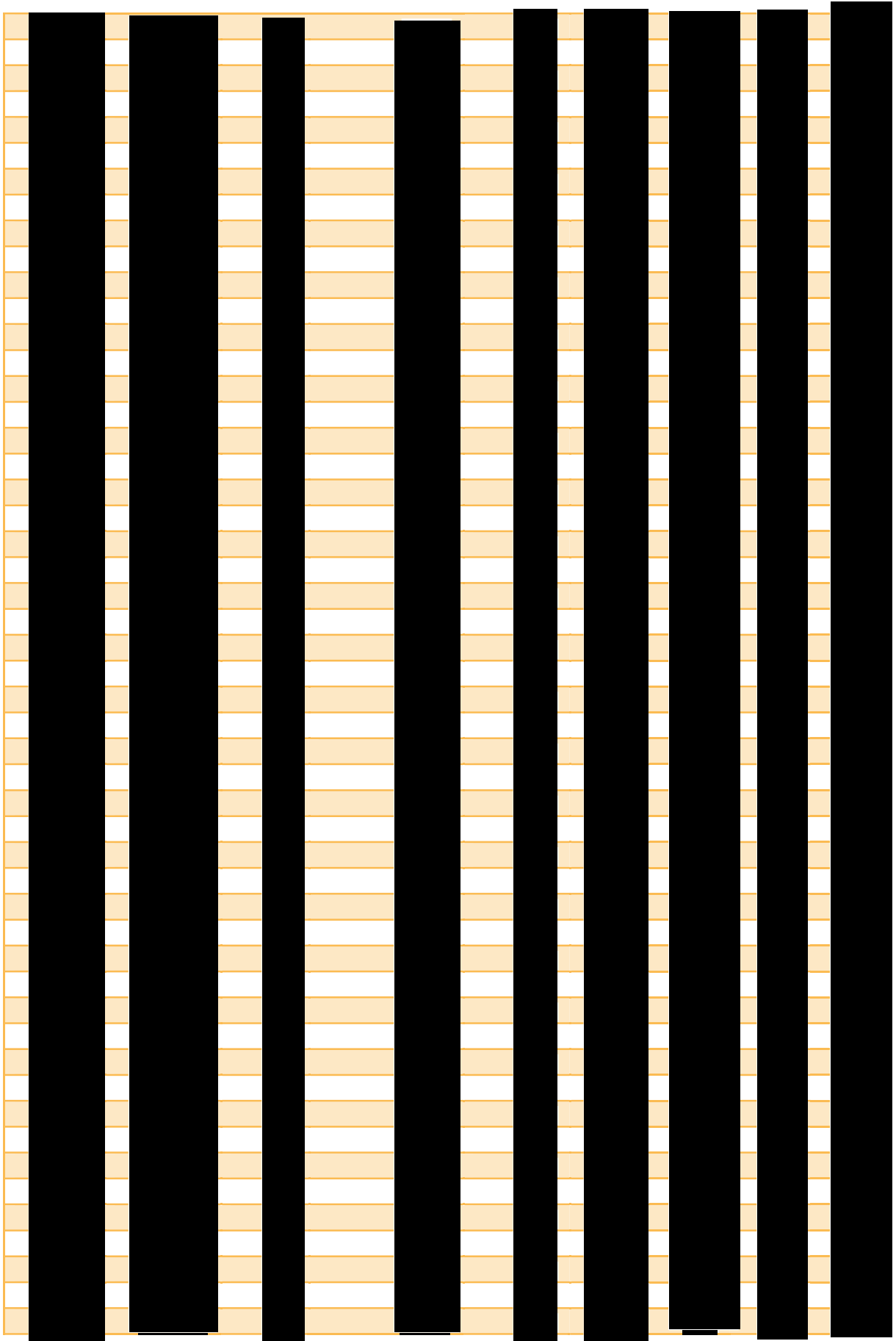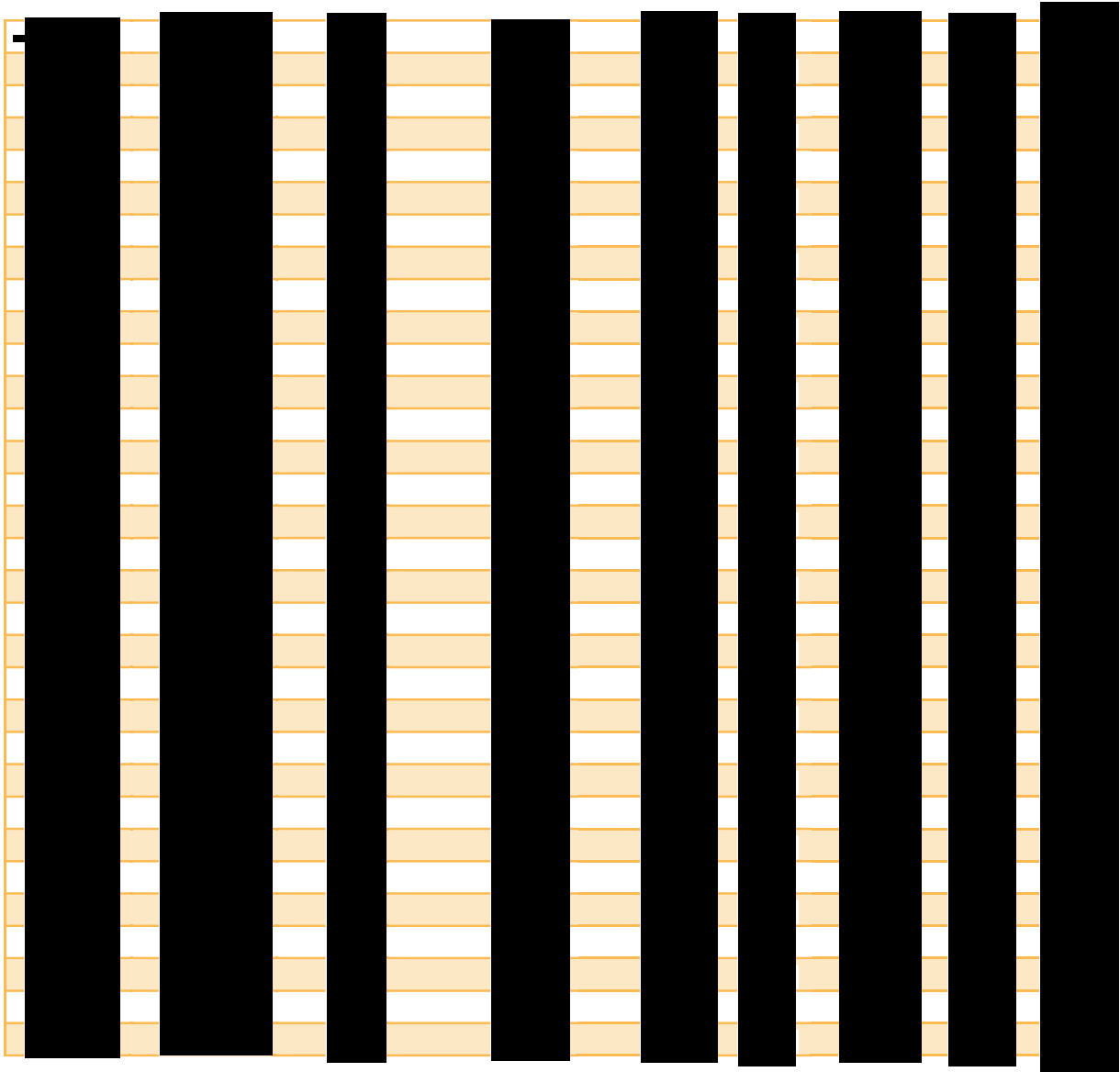
7.5.3. ███████ (Case 3)

A geographically referenced plot of ███████ is illustrated by Figure 46 and the predictions made for each WTG location are listed by Table 19.
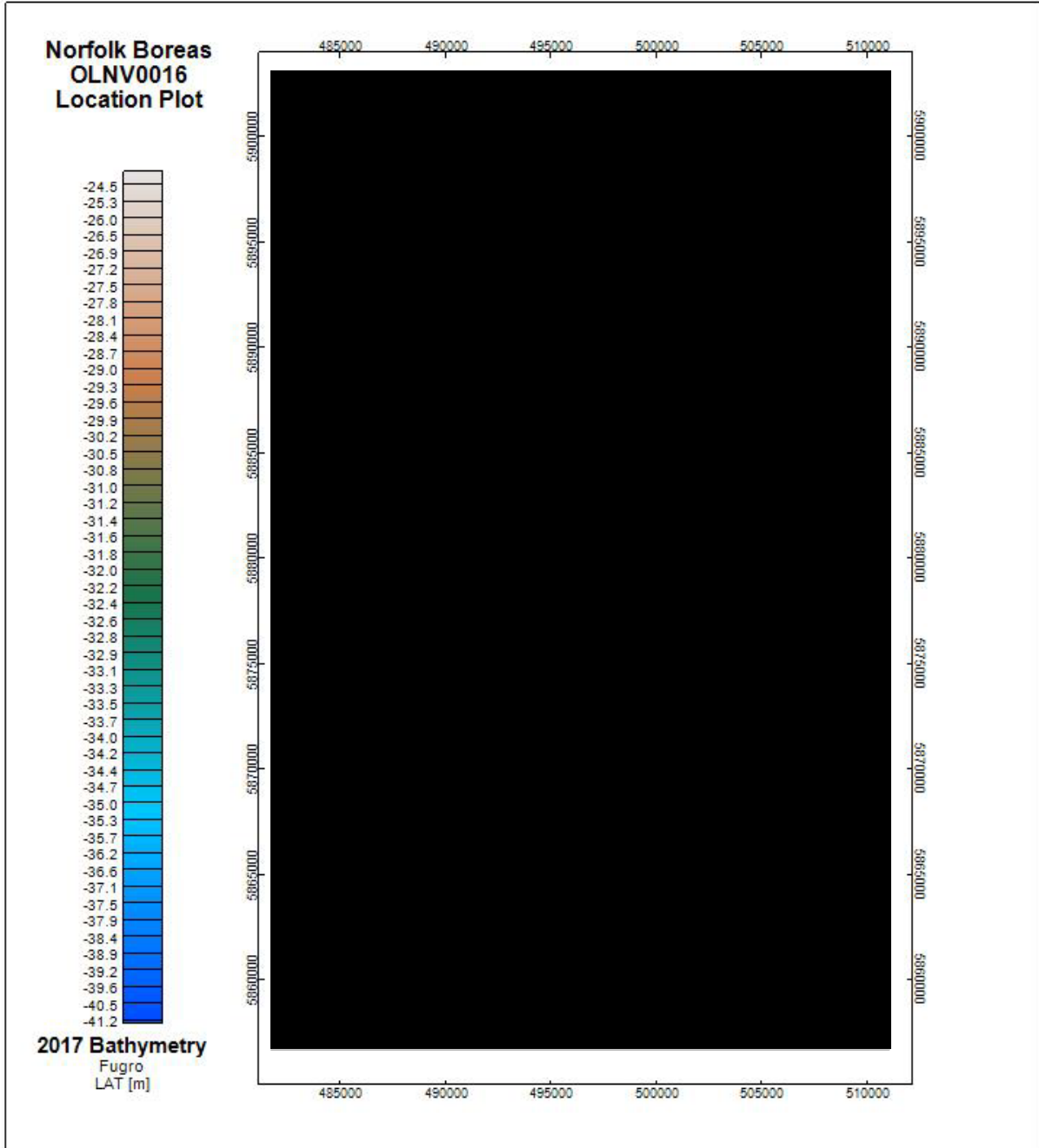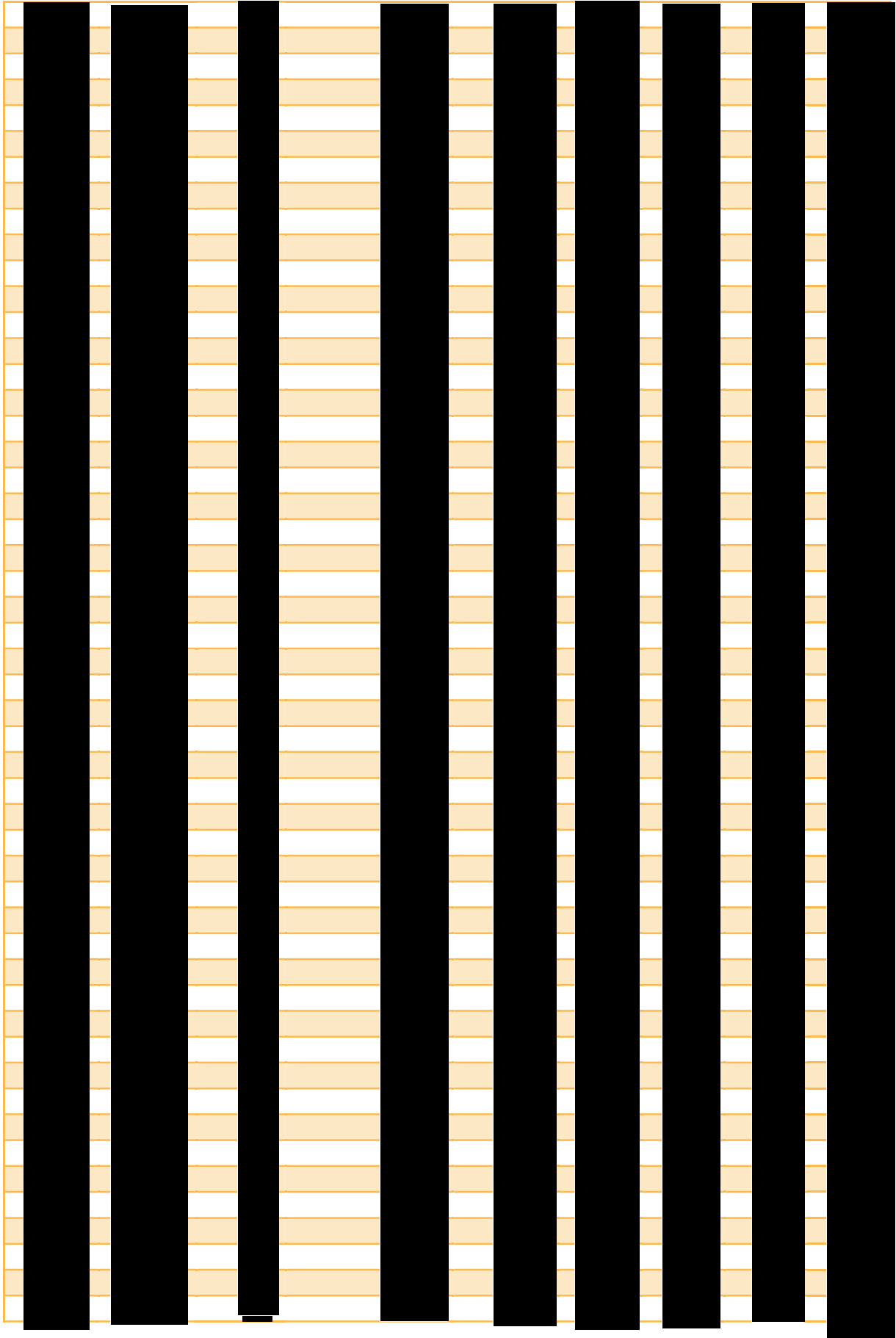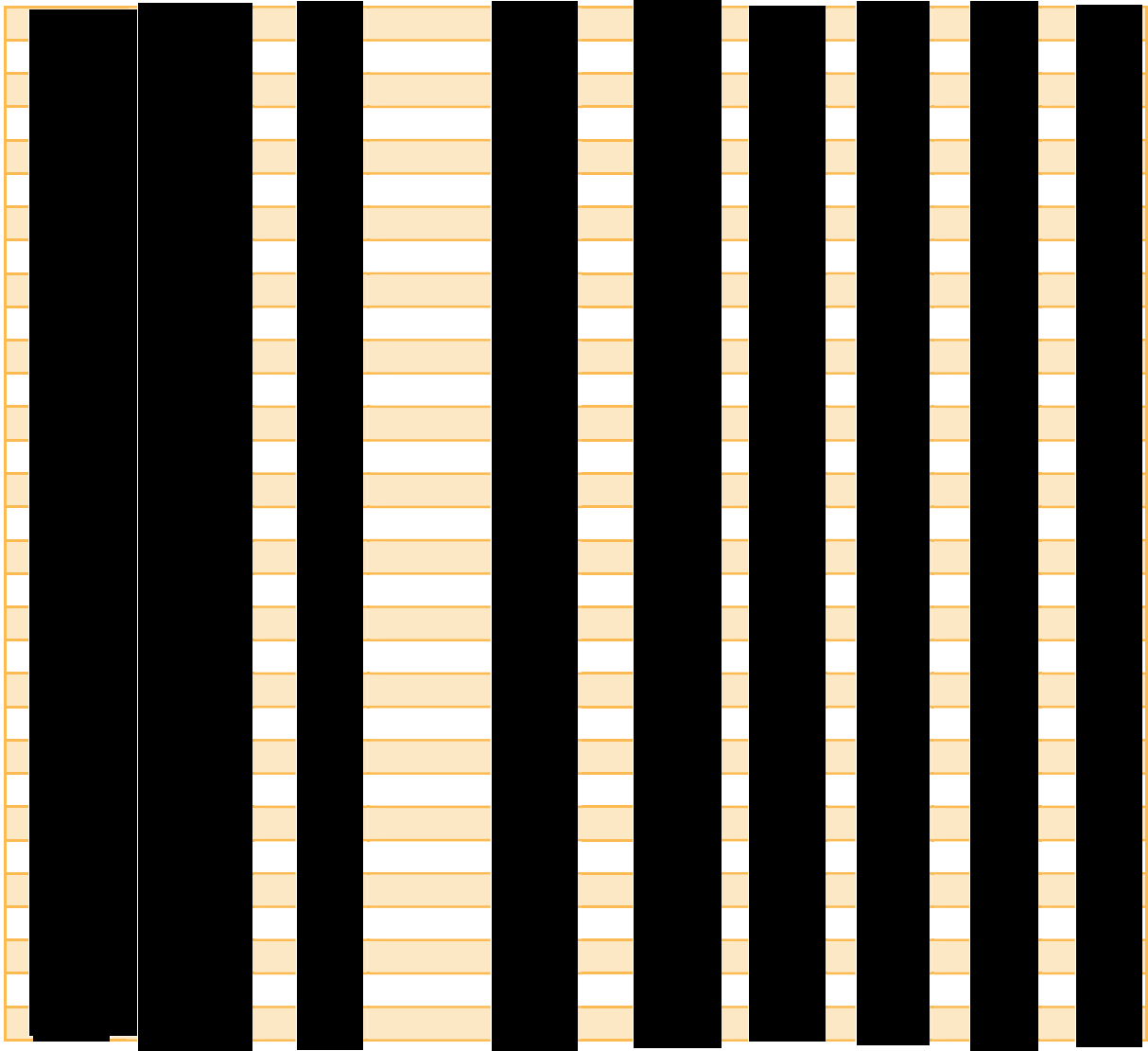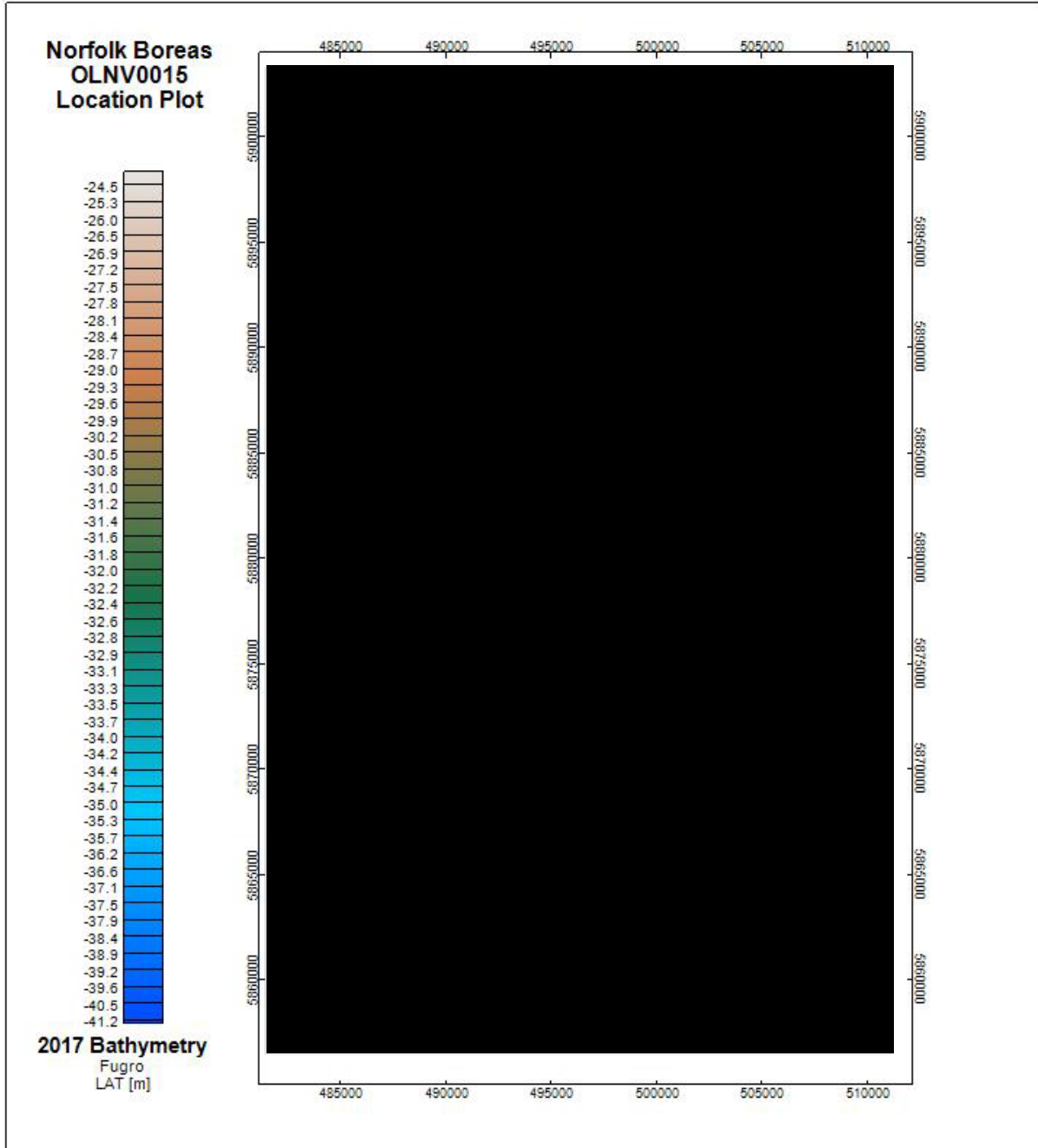

Figure 46: LNV026 Layout plot on Fugro 2017 Bathymetry

Table 19: Layout ▮▮▮▮▮ redictions for global seabed changes. Values in [m].

ETRS89 UTM31N		Turbine ID	Water depth (LAT [m])	Modelled Vertical Change [m]				
X	Y		Measured (2017)	2020	2025	2030	HSBL	LSBL

Norfolk Boreas - Geophysical Seabed mobility assessment
Morphodynamic study
Confidentiality class: High (C3)

Norfolk Boreas - Geophysical Seabed mobility assessment
Morphodynamic study

Confidentiality class: High (C3)

7.6. Layout summaries

The results shown in Section 7.5.1 to Section 7.5.3 are summarized in this section. To assess the number of critical positions for each layout, the classification scheme adopted by Deltares[18] (Table 20) was used. The results are shown in Table 21 - Table 23.

Table 20: Classification of seabed positions, table by Deltares. Un-recommended rephrased to "Not-recommended".
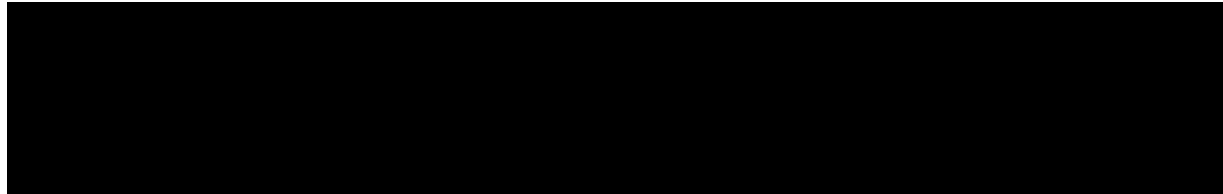
███

Table 21: Layout breakdown ████████

Assumption	Preferred	Possible	Better avoided	Un-recommended	Unknown
Best Estimate (2017 -2055)	115	8	5	2	0
Min/Max (2017 -2055)	104	14	8	4	0

Table 22: Layout breakdown ████████

Assumption	Preferred	Possible	Better avoided	Un-recommended	Unknown
Best Estimate (2017 -2055)	110	5	9	4	2
Min/Max (2017 -2055)	103	11	9	5	2

Table 23: Layout breakdown, ████████

Assumption	Preferred	Possible	Better avoided	Un-recommended	Unknown
Best Estimate (2017 -2055)	116	6	4	3	1
Min/Max (2017 -2057)	101	17	7	4	1

It can be identified from the tables above (Table 21 - Table 23), that in terms of best estimates most WTG positions are situated at preferred or possible locations. Some positions are considered not-recommended, and from a perspective of global scour should be re-evaluated for re-location.

7.7. Detailed Results

A list of attached (digital) supporting appendices is shown in this section.
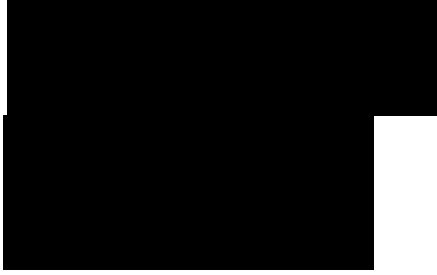
8. Future work

The model created based on the 2010 – 2017 time series has been reviewed and validated against available data. To further develop and validate the additional data acquired by Vattenfall will incorporated when available.

Validation and refinement (where appropriate) of the model should be completed when additional data becomes available. Updates will be detailed in technical notes.

The results detailed in this report are only valid for the layout used, therefore for each new layout or updated version of the existing layout the proposed WTG locations should be assessed. It is recommended that a site-specific set of zones relating to differing levels of seabed mobility is developed for WTG foundations and cables. Recommendations are based on generic foundation designs at present, as such once site-specific foundation designs are available the details of the report should be updated.

9. Conclusion

The Norfolk Boreas Wind Farm Zone exhibits significant morphodynamic features, which primarily migrate in directions coincident with the dominant residual tidal currents flowing ~357 - 334° NNW. The most prominent features being sand-waves (wave-lengths in excess of 100m and amplitudes exceeding 3m) with superimposed mega-ripples (amplitudes < 0.5 m and wave lengths < 100m).

Each of the proposed wind farm layouts (██████████████████ and █████████) introduce unique positions requiring an individual assessment at each WTG location.

Using the best estimate model results, most WTG positions for the wind farm layouts which were evaluated for this report, were situated at 'preferred' or "possible" areas throughout the site. Even in the most extreme cases considered (minimum / maximum predicted seabed levels) only some positions are considered "Better avoided" or "not-recommended".

10. References

1. Fugro, B. V. *Norfolk Vanguard Offshore Wind Farm, Geophysical Investigation Report - Geophysical Site Survey*. **2,** (2016).
2. Allen, J. R. L. *Sedimentary Structures - Their characteristics and physical basis*. (Elsevier, 1982).
3. Reynolds_International. *Re-processing and re-interpretation of Sub-Bottom Profiling data and development of a Ground Model for the East Anglia North zone*. **2,** (2015).
4. Fugro. *Norfolk Boreas Offshore Wind Farm Geophysical Site Investigation - Interpretive Site Investigation Report*. **2,** (2018).
5. Fugro, B. V. *Technical Note Seabed Mobility Survey Norfolk Vanguard & Boreas Offshore Wind Farms*. (2018).
6. Vattenfall. Norfolk Vanguard Geo Model. 31 (2018).
7. Fugro, B. V. *Technical Note Met Mast ZE Site Survey Norfolk Boreas Offshore Wind Farm*. (2017).
8. Deltares. East Anglia Offshore Wind Farm - Metocean Study. **1.1,** 74 (2012).
9. Partrac. Seabed Mobility at the East Anglia One Site. 1–49 (2014).
10. Fugro. *Norfolk Vanguard Offshore Wind Farm UK Continental Shelf , North Sea Report 2 of 3 : Geotechnical Investigation Report - Measured and Derived Geotechnical Parameters and Final Results*. **2,** (2017).
11. Fugro. *Norfolk Boreas Offshore Wind Farm United Kingdom Continental Shelf , Geotechnical Site Investigation Laboratory Test*. **3,** (2018).
12. DNV-GL. DNVGL-ST-0437: Loads and site conditions for wind turbines. (2016).
13. DNV-GL. DNVGL-ST-0126: Support Structures For Wind Turbines. (2016).
14. DNV-GL. DNVGL-SE-0190 - Project certification of wind power plants. 86 (2015).
15. Stoker, M. S., Balson, P. S., Long, D. & Tappin, D. R. An overview of the lithostratigraphical framework for the Quaternary deposits on the United Kingdom continental shelf. *Br. Geol. Surv. Res. Rep.* **RR/11/03,** 48 (2011).
16. Damen, J. M., van Dijk, T. A. G. P. & Hulscher, S. J. M. H. Spatially Varying Environmental Properties Controlling Observed Sand Wave Morphology. *J. Geophys. Res. Earth Surf.* **123,** 262–280 (2018).
17. Venditti, J. G., Church, M. & Bennett, S. J. Morphodynamics of small-scale superimposed sand waves over migrating dune bed forms. *Water Resour. Res.* **41,** (2005).
18. Deltares. *Morphodynamics of Hollandse Kust (zuid) Wind Farm Zone*. 100 (2016).
19. Zeiler, M., Schwarzer, K. & Ricklefs, K. Seabed morphology and sediment dynamics. *Kuste* 31–44 (2008).
20. Németh, A. A., Hulscher, S. J. M. H. & De Vriend, H. J. Modelling sand wave migration in shallow shelf seas. *Cont. Shelf Res.* **22,** 2795–2806 (2002).
21. Blondeaux, P. Sediment mixtures, coastal bedforms and grain sorting phenomena: An overview of the theoretical analyses. *Advances in Water Resources* **48,** 113–124 (2012).
22. Schwarzacher, W. Repetitions and cycles in stratigraphy. *Earth Sci. Rev.* **50,** 51–75 (2000).
23. Christie-Blick, N. Onlap, offlap, and the origin of unconformity-bounded depositional sequences. *Mar. Geol.* **97,** 35–56 (1991).
24. Zecchin, M. & Catuneanu, O. High-resolution sequence stratigraphy of clastic shelves

I: Units and bounding surfaces. *Mar. Pet. Geol.* **39,** 1–25 (2013).

25. Catuneanu, O. *et al.* Towards the standardization of sequence stratigraphy. *Earth-Science Rev.* **92,** 1–33 (2009).

26. Catuneanu, O. Principles of Sequence Stratigraphy. *Changes* 375 (2006). doi:10.5860/CHOICE.44-4462

27. Miall, A. D. Sequence stratigraphy and chronostratigraphy: problems of definiton and precison in correlation, and their implications for global eustasy. *Geosci. Canada* **21,** 1–26 (1994).

28. Miller, K. G. *et al.* Cenozoic global sea level, sequences, and the New Jersey transect: Results from coastal plain and continental slope drilling. *Rev. Geophys.* **36,** 569–601 (1998).

29. Helland-Hansen, W. & Gjelberg, J. G. Conceptual basis and variability in sequence stratigraphy: a different perspective. *Sediment. Geol.* **92,** 31–52 (1994).

30. Sylvester, Z., Pirmez, C. & Cantelli, A. A model of submarine channel-levee evolution based on channel trajectories: Implications for stratigraphic architecture. *Mar. Pet. Geol.* **28,** 716–727 (2011).

31. Clausen, O. R., Śliwińska, K. K. & Gołedowski, B. Oligocene climate changes controlling forced regression in the eastern North Sea. *Mar. Pet. Geol.* **29,** 1–14 (2012).

32. Vattenfall. VKF-VHN-CID-DD-0039-VHN Geophysical Seabed mobility assessment rev 2. 75 (2017).

33. van Oyen, T. & Blondeaux, P. Grain sorting effects on the formation of tidal sand waves. *J. Fluid Mech.* **629,** 311 (2009).

34. Lanckneus, J. & De Moor, G. Present-day evolution of sand waves on a sandy shelf bank. *Oceanol. Acta* **11,** 123–127 (1991).

35. Nichols, G. *Sedimentology and Stratigraphy.* (Wiley-Blackwell, 2009).

36. Berg, J. Van Den. A simplified sand wave model. 284–289 (2004).

37. Borsje, B. W., Roos, P. C., Kranenburg, W. M. & Hulscher, S. J. M. H. Modeling tidal sand wave formation in a numerical shallow water model: The role of turbulence formulation. *Cont. Shelf Res.* **60,** 17–27 (2013).

38. Michelsen, O. & Sørensen, J. a N. C. Upper Cenozoic sequences in the southeastern North Sea Basin. *Bulletin of the Geological Society of Denmark* **42,** 74–95 (1998).

39. Pedersen, S. Architecture of Glaciotectonic Complexes. *Geosciences* **4,** 269–296 (2014).

40. Nielsen, S. B. *et al.* The ICE hypothesis stands: How the dogma of late Cenozoic tectonic uplift can no longer be sustained in the light of data and physical laws. *J. Geodyn.* **50,** 102–111 (2010).

41. Kaskela, A. M., Kotilainen, A. T., Al-Hamdani, Z., Leth, J. O. & Reker, J. Seabed geomorphic features in a glaciated shelf of the Baltic Sea. *Estuar. Coast. Shelf Sci.* **100,** 150–161 (2012).

42. Rasmussen, E. S. The interplay between true eustatic sea-level changes, tectonics, and climatic changes: What is the dominating factor in sequence formation of the Upper Oligocene-Miocene succession in the eastern North Sea Basin, Denmark? *Glob. Planet. Change* **41,** 15–30 (2004).

43. Ballantyne, C. K. Paraglacial geomorphology. *Quaternary Science Reviews* **21,** 1935–2017 (2002).

44. Cazenave, A. *et al.* The rate of sea-level rise. *Nat. Clim. Chang.* **4,** 358–361 (2014).

45. Fugro. *Norfolk Boreas Offshore Wind Farm, Geotechnical Site Investigation, Investigation Data Report.* **2,** (2017).

46. Fugro. *Geotechnical Report Soil Parameter Values Norfolk Vanguard Offshore Wind*

      Farm Geotechnical Report Soil Parameter Values Norfolk Vanguard Offshore Wind Farm UK Sector , North Sea. (2017).

47.   Eecen, P. J. Current Profiles at the Offshore Wind Farm Egmond aan Zee. (2010).

48.   Briggs, K. B., Lyons, A. P., Pouliquen, E., Mayer, L. A. & Richardson, M. D. Seafloor roughness, sediment grain size, and temporal stability. in *Underwater Acoustic Measurements: Technologies & Results* 8 (2005).

49.   Gardline. *East Anglia Offshore Wind, Geophysical Survey, Area A*. **1,** (2010).

50.   Gardline. *East Anglia Offshore Wind, Geophysical Survey Area B*. **1,** (2010).

51.   Report, C. & Wind, V. *Fugro Norfolk Boreas Offshore Wind Farm UK Continental Shelf , North Sea Report 1 of 3 : Geophysical Site Investigation, Operations and Calibrations Report*. **1 of 2,** (2017).

52.   Jones, C. Vertical Offshore Reference Frame (VORF). 1 (2007).

53.   IHO. IHO Standards for Hydrographic Surveys. **5,** 36 (2008).

54.   Vattenfall Vindkraft A/S. Scope of Work, East Anglia North Offshore Windfarm, Geophysical Site Investigation Survey. 50 (2016).

55.   Smith, W. H. F. & Wessel, P. Gridding with continuous curvature splines in tension. *Geophysics* **55,** 293–305 (1990).

56.   Klahn, M. VKF-VHS-CID-DD-0043-VHS Geophysical Seabed mobility assessment_rev_1. 77 (2017).

57.   Voepel, H., Schumer, R. & Hassan, M. A. Sediment residence time distributions: Theory and application from bed elevation measurements. *J. Geophys. Res. Earth Surf.* **118,** 2557–2567 (2013).

58.   Tacher, L., Pomian-Srzednicki, I. & Parriaux, A. Geological uncertainties associated with 3-D subsurface models. *Comput. Geosci.* **32,** 212–221 (2006).

59.   Rood, R. B. Test plans for geophysical modeling. 16 (2018).

60.   Denton, N. *Seabed and Sub-Seabed Data Required for Approvals of Mobile Offshore Units (MOU)*. **8,** 16 (2015).